



Since January 2020 Elsevier has created a COVID-19 resource centre with free information in English and Mandarin on the novel coronavirus COVID-19. The COVID-19 resource centre is hosted on Elsevier Connect, the company's public news and information website.

Elsevier hereby grants permission to make all its COVID-19-related research that is available on the COVID-19 resource centre - including this research content - immediately available in PubMed Central and other publicly funded repositories, such as the WHO COVID database with rights for unrestricted research re-use and analyses in any form or by any means with acknowledgement of the original source. These permissions are granted for free by Elsevier for as long as the COVID-19 resource centre remains active.



A lipid nanoparticle platform for mRNA delivery through repurposing of cationic amphiphilic drugs

Bram Bogaert^a, Félix Sauvage^a, Roberta Guagliardo^a, Cristina Muntean^a, Van Phuc Nguyen^b, Eline Pottie^c, Mike Wels^a, An-Katrien Minnaert^a, Riet De Rycke^d, Qiangbing Yang^e, Dan Peer^f, Niek Sanders^g, Katrien Remaut^a, Yannis M. Paulus^b, Christophe Stove^c, Stefaan C. De Smedt^a, Koen Raemdonck^{a,*}

^a Ghent Research Group on Nanomedicines, Laboratory of General Biochemistry and Physical Pharmacy, Faculty of Pharmaceutical Sciences, Ghent University, Ottergemsesteenweg 460, 9000 Ghent, Belgium

^b Department of Ophthalmology and Visual Sciences, University of Michigan, Ann Arbor, MI, USA

^c Laboratory of Toxicology, Faculty of Pharmaceutical Sciences, Ghent University, Ottergemsesteenweg 460, 9000 Ghent, Belgium

^d Ghent University Expertise Center for Transmission Electron Microscopy and VIB BioImaging Core, 9052 Ghent, Belgium

^e Experimental Cardiology Laboratory, Regenerative Medicine Center Utrecht and Circulatory Health Laboratory, University Medical Center Utrecht, University Utrecht, Heidelberglaan 100, Utrecht, the Netherlands

^f Laboratory of Precision NanoMedicine, Shmunis School of Biomedicine and Cancer Research, Tel-Aviv University, Ramat Aviv, Tel-Aviv 69978, Israel

^g Laboratory of Gene Therapy, Faculty of Veterinary Medicine, Ghent University, Heidestraat 19, 9820 Merelbeke, Belgium

ARTICLE INFO

Keywords:

Nanomedicine
Drug repurposing
Cationic amphiphilic drugs
Messenger RNA
RNA therapeutics
Lipid nanoparticles
Cellular delivery

ABSTRACT

Since the recent clinical approval of siRNA-based drugs and COVID-19 mRNA vaccines, the potential of RNA therapeutics for patient healthcare has become widely accepted. Lipid nanoparticles (LNPs) are currently the most advanced nanocarriers for RNA packaging and delivery. Nevertheless, the intracellular delivery efficiency of state-of-the-art LNPs remains relatively low and safety and immunogenicity concerns with synthetic lipid components persist, altogether rationalizing the exploration of alternative LNP compositions. In addition, there is an interest in exploiting LNP technology for simultaneous encapsulation of small molecule drugs and RNA in a single nanocarrier. Here, we describe how well-known tricyclic cationic amphiphilic drugs (CADs) can be repurposed as both structural and functional components of lipid-based NPs for mRNA formulation, further referred to as CADosomes. We demonstrate that selected CADs, such as tricyclic antidepressants and antihistamines, self-assemble with the widely-used helper lipid DOPE to form cationic lipid vesicles for subsequent mRNA complexation and delivery, without the need for prior lipophilic derivatization. Selected CADosomes enabled efficient mRNA delivery in various *in vitro* cell models, including easy-to-transfect cancer cells (e.g. human cervical carcinoma HeLa cell line) as well as hard-to-transfect primary cells (e.g. primary bovine corneal epithelial cells), outperforming commercially available cationic liposomes and state-of-the-art LNPs. In addition, using the antidepressant nortriptyline as a model compound, we show that CADs can maintain their pharmacological activity upon CADosome incorporation. Furthermore, *in vivo* proof-of-concept was obtained, demonstrating CADosome-mediated mRNA delivery in the corneal epithelial cells of rabbit eyes, which could pave the way for future applications in ophthalmology. Based on our results, the co-formulation of CADs, helper lipids and mRNA into lipid-based nanocarriers is proposed as a versatile and straightforward approach for the rational development of drug combination therapies.

* Corresponding author.

E-mail addresses: Bram.Bogaert@UGent.be (B. Bogaert), Felix.Sauvage@UGent.be (F. Sauvage), Roberta.Guagliardo@UGent.be (R. Guagliardo), Cristina.Muntean@UGent.be (C. Muntean), vanphucn@med.umich.edu (V.P. Nguyen), Eline.Pottie@UGent.be (E. Pottie), Mike.Wels@UGent.be (M. Wels), AnKatrienPaula.Minnaert@UGent.be (A.-K. Minnaert), Riet.DeRycke@UGent.be (R. De Rycke), q.yang@umcutrecht.nl (Q. Yang), peer@tauex.tau.ac.il (D. Peer), Niek.Sanders@UGent.be (N. Sanders), Katrien.Remaut@UGent.be (K. Remaut), ypaulus@med.umich.edu (Y.M. Paulus), Christophe.Stove@UGent.be (C. Stove), Stefaan.Desmedt@UGent.be (S.C. De Smedt), Koen.Raemdonck@UGent.be (K. Raemdonck).

<https://doi.org/10.1016/j.jconrel.2022.08.009>

Received 21 October 2021; Received in revised form 3 August 2022; Accepted 5 August 2022

Available online 24 August 2022

0168-3659/© 2022 Published by Elsevier B.V.

1. Introduction

Nucleic acid therapeutics are an emerging class of drugs that address diseases at the genomic and/or transcriptomic level [1,2]. For example, small interfering RNA (siRNA) and messenger RNA (mRNA) both enable regulation of intracellular protein concentrations. Following cytosolic delivery, siRNAs activate the RNA interference (RNAi) pathway, leading to sequence-specific silencing of genes at the post-transcriptional level, while delivery of *in vitro* transcribed mRNA can drive expression of therapeutic proteins and antigens [3–6]. To overcome the many extra- and intracellular barriers upon *in vivo* administration, including nuclease degradation, tissue distribution and delivery across cellular membranes, RNA therapeutics are typically encapsulated in synthetic nanoparticles (NPs) [7,8]. Among the various NPs under investigation, lipid nanoparticles (LNPs) currently are the preferred carrier material for RNA delivery [9]. LNPs generally contain one or more helper lipids (e.g. DOPE, DSPC, cholesterol, etc.) and a cationic or ionizable lipid, the latter being responsible for electrostatic complexation of the oppositely charged RNA and subsequent endosomal escape [10–12]. A recent milestone for the RNA drug delivery field was achieved in August 2018, when the first RNAi-based medicinal product Onpatro® (patisiran), i.e. an LNP formulation containing the ionizable lipid DLin-MC3-DMA, was approved by the US Food and Drug Administration, shortly followed by the European Medicines Agency [13,14]. Additionally, the recent approval of the LNP-based COVID-19 mRNA vaccines of both Pfizer/BioNTech and Moderna against SARS-Cov-2 highlight the great potential of mRNA for prophylaxis of infectious diseases. Moreover, it is believed that the success of the mRNA vaccines could accelerate therapeutic applications for mRNA [15–20].

Various types of cationic lipids, ionizable lipids and lipid-like molecules have been designed with diverging physicochemical properties for LNP formulation [21–25]. However, despite the great promise for RNA therapeutics, even for state-of-the-art LNPs intracellular delivery often remains inefficient, with only 1–4% of the endocytosed RNA dose actually escaping the endosomal confinement to reach the cytosol [22,26–28]. In addition, besides facilitating RNA encapsulation and cellular delivery, synthetic lipids do not always have desirable biological activity. Indeed, cellular toxicity and immunogenicity are major potential drawbacks associated with the use of cationic LNPs, especially when repeated administration is required [9,29–33]. As such, alternative materials should be considered that enable sufficient cytosolic release of the encapsulated RNA with acceptable cellular toxicity.

Recent studies from our laboratory have successfully shown that widely used cationic amphiphilic drugs (CADs) can be repurposed as small nucleic acid delivery enhancers [34,35,67]. CADs are pharmacologically diverse compounds (e.g. antidepressants, antihistamines, anti-hypertensives) that tend to accumulate in acidified lysosomes given their amphiphilic and weak basic properties, leading to functional acid sphingomyelinase (ASM) inhibition. As a result, CADs transiently induce an acquired lysosomal storage disease phenotype, with typical hallmarks such as (phospho)lipidosis, lysosomal swelling and lysosomal membrane permeabilization (LMP), the latter facilitating the release of decomplexed siRNAs into the cytosol. Combining CADs with RNA drugs can be considered as a dose sparing strategy, reducing the required dose of an siRNA-loaded NP to achieve sufficient knockdown of a disease-causing gene. Furthermore, the intrinsic pharmacological effect of the CAD could contribute to the envisioned therapeutic response. A drug repurposing screen of the National Institutes of Health Clinical Collection compound library (NIHCC) identified 56 CADs from various drug classes that significantly enhanced siRNA delivery when applied sequentially to NP-transfected cells, indicating that many CADs share this delivery-promoting effect independent of their underlying pharmacological activity [36]. However, it was also observed that the CAD-induced pore size in the lysosomal limiting membrane does not allow endolysosomal escape of larger RNA cargo, precluding the extrapolation of this drug delivery concept to mRNA therapeutics [35,36].

To enable merging CAD pharmacological activity with mRNA delivery, in this work we aimed to exploit CADs as both structural and functional components of mRNA LNPs. It is hypothesized that the typical physicochemical features of CADs and their known tendency to insert in lipid membranes would allow their incorporation into LNPs for mRNA complexation, thus replacing potentially harmful synthetic cationic lipids. Moreover, CADs have been described to modify lipid bilayer properties, which could promote RNA delivery efficiency [37–40]. Finally, incorporating both CADs and mRNA into LNPs should enable to merge the therapeutic activities of both drugs in a single formulation [41]. To this end, a selection of CADs, including the tricyclic antidepressant nortriptyline (NT), was screened in combination with 1,2-dioleoyl-sn-glycero-3-phosphoethanolamine (DOPE) as a fusogenic helper lipid for their ability to form stable complexes with mRNA, further referred to as CADosomes. Extensive physicochemical characterization provided insight into CADosome structure, morphology as well as mRNA complexation efficiency. Next, CADosome-mediated functional delivery of mRNA was evaluated in various *in vitro* cell models, including easy-to-transfect cancer cells (e.g. human cervical carcinoma HeLa cell line) as well as hard-to-transfect primary cells (e.g. primary bovine corneal epithelial cells (PBCECs)). Furthermore, the CAD pharmacological activity when incorporated in CADosomes was probed by quantifying the antagonistic effect of NT at the G protein-coupled serotonin 2A receptor (5-HT_{2A}R), via β -arrestin 2 recruitment in a Nanoluciferase Binary Technology (NanoBiT®) cellular assay. Finally, *in vivo* eGFP expression was quantified following CADosome deposition on the cornea of rabbits. Our data indicate that selected CADs (e.g. tricyclic antidepressants and antihistamines) and mRNA therapeutics can be successfully co-encapsulated into LNPs with the fusogenic helper lipid DOPE without the need for state-of-the-art cationic or ionizable lipids. Moreover, CADs maintain their pharmacological effect upon LNP incorporation and enable functional mRNA delivery in different *in vitro* cell models as well as *in vivo* in the corneal epithelial cells of rabbit eyes, providing opportunities for drug combination therapy.

2. Results and discussion

2.1. Preparing CADosomes using the tricyclic antidepressant nortriptyline as structural component

Previous work has illustrated that sequential administration of CADs to NP-transfected cells facilitates cytosolic delivery of small RNA therapeutics (e.g. siRNA) but not their larger counterparts (e.g. mRNA) [35,36]. Here, we evaluated if CADs can be harnessed as structural and functional components of LNPs for mRNA complexation and delivery. With their charged headgroup, CADs can interact with anionic phosphatidylserine membranes via coulomb- or ion-induced dipole interactions, while zwitterionic phosphatidylcholine and phosphatidylethanolamine domains are mainly reached by Van der Waals forces and hydrophobic effects. In particular, tricyclic antidepressants (TCA) are well known to partition in lipid bilayers [38,39]. It is described that TCAs insert within lipid membranes via their hydrophobic aromatic rings while the polar side chains, including charged amine groups, are localized near the phospholipid headgroups [37]. As such, the TCA nortriptyline hydrochloride (NT) (clogP 4.51 and pKa 10.1) was initially used as model CAD molecule to explore NP formation in combination with the widely used helper lipid DOPE [29,42–44]. Stable and cationic vesicles could be obtained by simply mixing NT with DOPE (50:50 molar ratio), indicating their self-assembly, both via ethanol dilution and lipid film hydration methods, as schematically illustrated in Fig. 1A [45–47]. Lipid film hydration followed by sonication resulted in smaller NT-DOPE vesicles of ~80 nm (PDI 0.2) with lower zeta potential (~ +20 mV) compared to ethanol dilution (~200 nm (PDI 0.2) and +25 mV). However, relative to conventional cationic DOTAP-DOPE liposomes (83 nm (PDI 0.3) and +50 mV) both NT-DOPE vesicles were substantially less positively charged (Fig. 1C, D and E). In a next step,

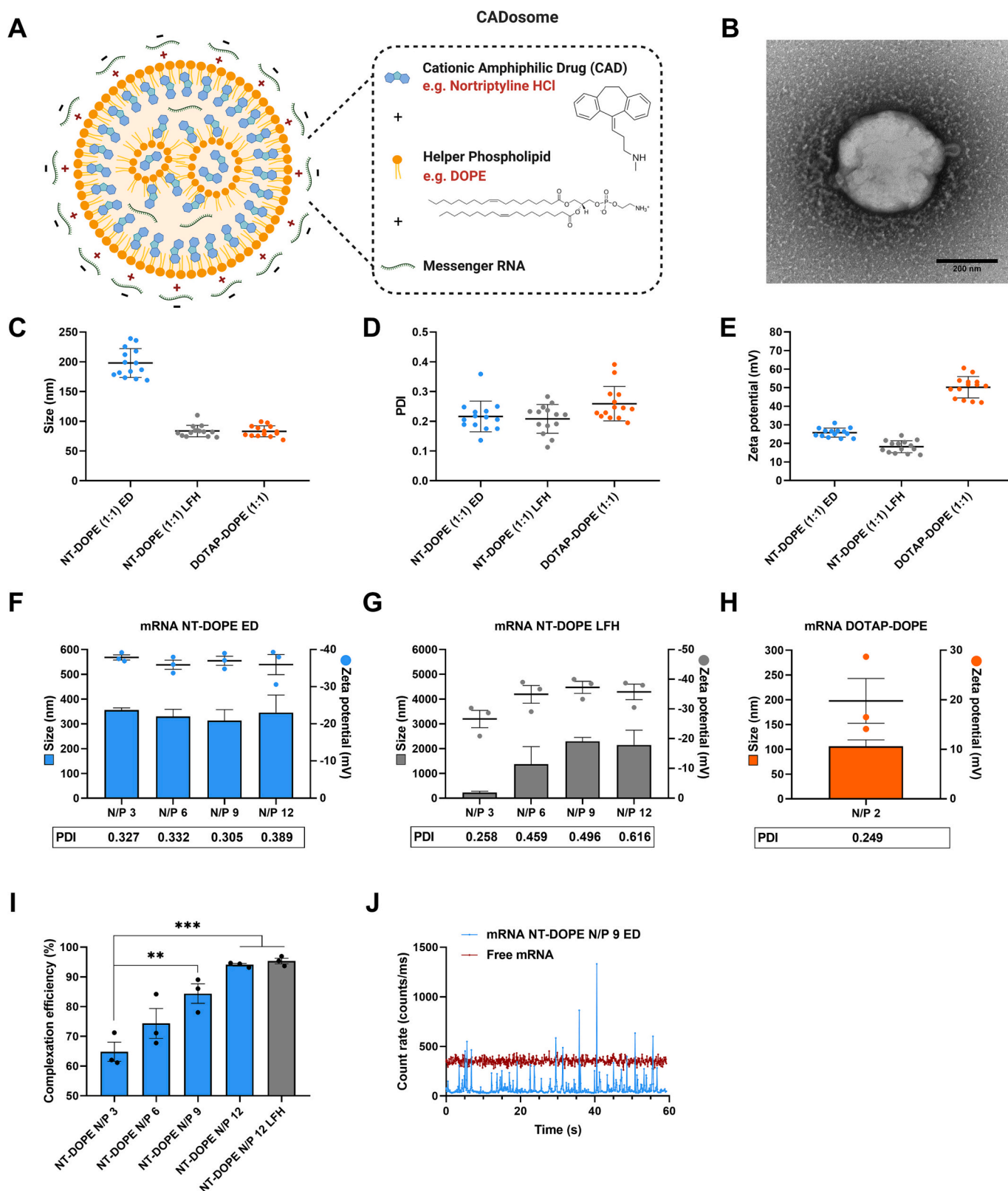


Fig. 1. Physicochemical characterization of mRNA CADosomes containing nortriptyline (NT)-DOPE (A) Schematic representation of NT-DOPE mRNA CADosomes, produced with vesicles obtained via an ethanol dilution (ED) or lipid film hydration (LFH) method. Created with BioRender.com (B) Representative transmission electron microscopy (TEM) image of enhanced green fluorescent protein-encoding messenger RNA (eGFP-mRNA) NT-DOPE CADosomes, prepared via ED. Scale bar corresponds to 200 nm. Dynamic light scattering data (hydrodynamic size, polydispersity index (PDI) and zeta potential) of NT-DOPE and DOTAP-DOPE vesicles, (C–E) prior to ($n = 14$) and (F–H) after complexation with eGFP-mRNA ($n = 3$). (I–J) Fluorescence correlation spectroscopy (FCS) analysis of CADosome mRNA complexation efficiency with different N/P ratios. Data are represented as mean \pm the standard error of the mean (SEM) for minimum three independent repeats ($n \geq 3$). Statistical analysis was performed using One Way Anova with Tukey Correction (** $p \leq 0.01$, *** $p \leq 0.001$). (For interpretation of the references to color in this figure legend, the reader is referred to the web version of this article.)

these vesicles were used for complexation of enhanced green fluorescent protein-encoding messenger RNA (eGFP-mRNA) at mounting nitrogen-to-phosphate (N/P) ratios to form NT-DOPE mRNA complexes further referred to as CADosomes (Fig. 1F, G and H). Transmission electron microscopy (TEM) typically showed spherical CADosomes with a dense lipid core (Fig. 1B and Fig. S1). CADosomes slightly increased in size when using ethanol dilution-derived NT-DOPE vesicles for mixing with mRNA, while the NT-DOPE vesicles obtained via lipid film hydration aggregated after mRNA complexation at all N/P ratios tested. Nevertheless, fluorescence correlation spectroscopy (FCS) analysis confirmed that up to 95% complexation efficiency could be reached at the highest N/P ratios (Fig. 1I and Fig. 1J) [48]. However, independent of the N/P ratio and vesicle preparation method, CADosomes shifted to a negative zeta potential, indicating that part of the mRNA strands is located on the outer surface of the complexes, while DOTAP-DOPE complexes remained positively charged at their most optimal N/P ratio [44]. Altogether, these data indicate that NT in combination with DOPE self-assembles into cationic vesicles with high mRNA complexation efficiency.

2.2. Exploring nortriptyline CADosomes for cytosolic mRNA delivery

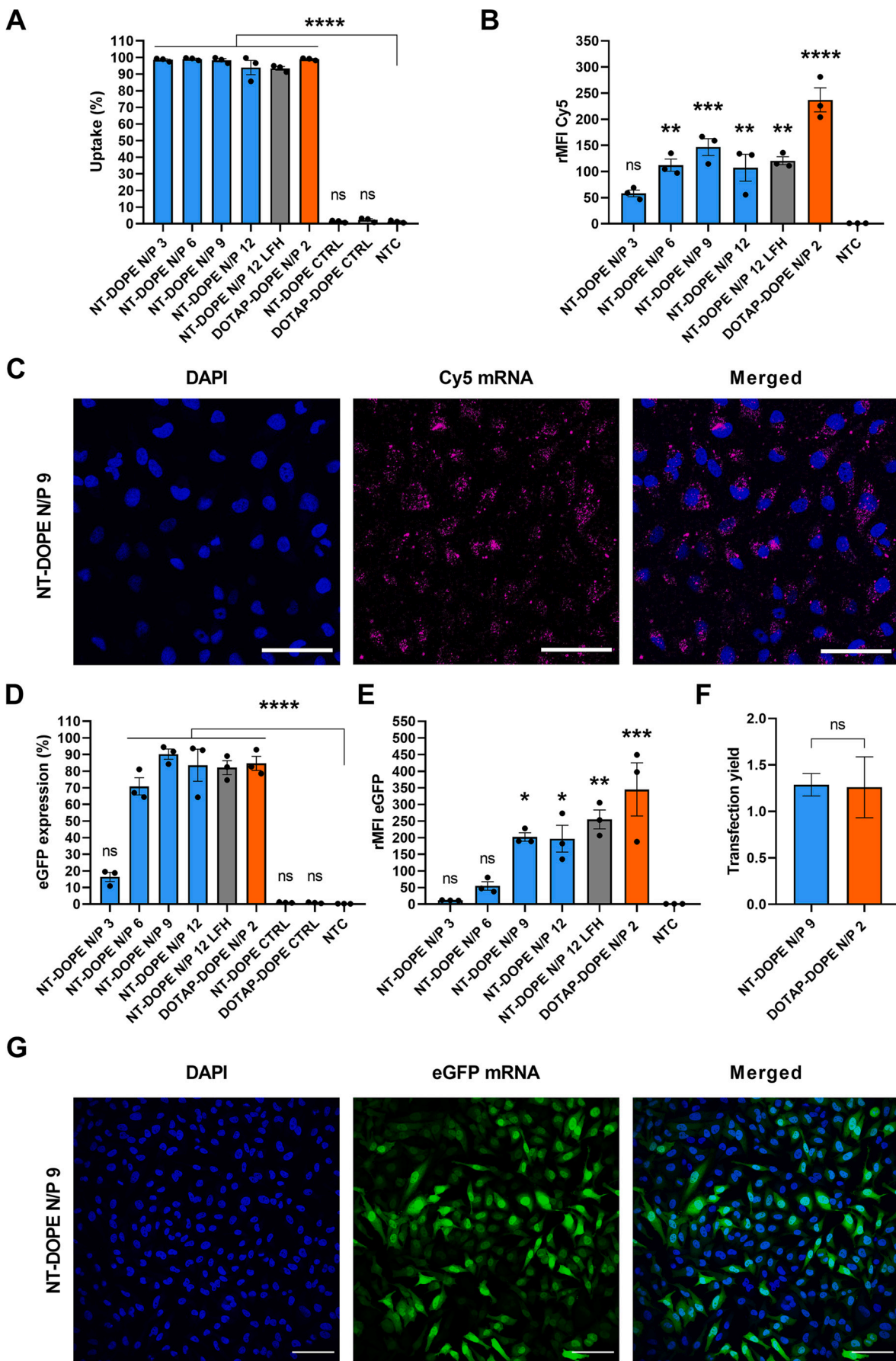
Having demonstrated that stable CADosomes could be formed with NT, we next aimed to evaluate *in vitro* mRNA delivery. Hereto, NT-DOPE CADosomes were first loaded with Cy5-labeled mRNA and their cellular uptake in HeLa cells was evaluated via confocal microscopy and flow cytometry (Fig. 2A–C and Fig. S2A). Independent of the NT-DOPE mRNA N/P ratio, >95% Cy5-positive cells was obtained (Fig. 2A). However, the relative mean fluorescence intensity (rMFI) compared to the non-treated control (NTC) was highest for CADosomes N/P 9, but remained significantly lower than DOTAP-DOPE (Fig. 2B). A possible explanation could be the difference in surface charge of both nanocarriers (Fig. 1F–H), where the negative zeta potential for the CADosomes is expected to reduce cell binding and internalization [49,50]. Confocal microscopy confirmed the internalization of Cy5-mRNA-loaded CADosomes in transfected HeLa cells (Fig. 2C). Next, mRNA-induced eGFP expression using CADosomes was determined 24 h post-transfection as a function of the N/P ratio and compared with cationic DOTAP-DOPE lipoplexes (N/P 2) (Fig. 2D–G). Up to 90% of the HeLa cells successfully expressed eGFP after transfection with CADosomes N/P 9 (Fig. 2D), which was visually confirmed via confocal microscopy (Fig. 2G and Fig. S2B). Furthermore, a higher N/P ratio correlated with a significant increase in eGFP expression (Fig. 2E). For the more stable CADosomes obtained via ethanol dilution, highest eGFP expression was observed for N/P 9, which was consequently selected as the most optimal composition. Of note, taking into account the lower cellular uptake of mRNA obtained via transfection with CADosomes, an equivalent mRNA transfection yield (*i.e.* eGFP expression normalized to the intracellular mRNA dose) was reached relative to the DOTAP-DOPE lipoplexes (Fig. 2F and Fig. S2C). It has been demonstrated in the literature that the helper lipid DOPE, containing a small phosphoethanolamine headgroup and two unsaturated oleoyl chains, displays a cone-like geometry that promotes the non-bilayer, inverse hexagonal (H_{II}) phase during endolysosomal membrane fusion or bilayer disruption [51–53]. Therefore, we hypothesize that upon cellular internalization DOPE contributes to the cytosolic delivery of mRNA via membrane fusion, while the CAD molecules are mainly responsible for mRNA complexation. A major difference with previously published work is that the CAD compounds do not need to be chemically modified to facilitate CADosome formation [41]. Lastly, a Cell-Titer-Glo® viability assay demonstrated acceptable cell viability for CADosomes N/P 3 to 9, while N/P 12 resulted in ~35% cell death (Fig. S3A), further supporting NT-DOPE CADosomes N/P 9 as the most optimal N/P ratio for further experiments.

2.3. Screening of CADosomes with diverging CADs for mRNA delivery in HeLa cells

To evaluate if our CADosome strategy for mRNA delivery could be extended to other CAD molecules, a small screen of selected CAD compounds based on our previous work (Table S1) were likewise mixed with DOPE (50:50 molar ratio) [36]. Ketotifen (clogP 3.35 and pKa 7.15), loperamide (clogP 4.77 and pKa 9.41), verapamil (clogP 5.04 and pKa 9.68) and epinastine (clogP 3.13 and pKa 9.31) did not self-assemble with DOPE to form stable nanosized cationic vesicles, neither via ethanol dilution nor lipid film hydration (data not shown). On the other hand, successful vesicle formation was achieved with amitriptyline hydrochloride (AMI) (clogP 4.81 and pKa 9.76), desipramine hydrochloride (DSI) (clogP 3.90 and pKa 10.02), imipramine hydrochloride (IMI) (clogP 4.28 and pKa 9.20), and desloratadine (DES) (clogP 3.97 and pKa 9.73), as illustrated in Fig. 3A. The latter CADs are structurally related to NT and are composed of an aromatic tricyclic domain with a three carbon tail substituted with secondary or tertiary methylated amine groups, or a heterocyclic amine piperidine group in case of desloratadine. This cationic lipid-like structure, with clearly segregated hydrophobic and charged amine moieties, could explain this self-assembly behavior with DOPE, in contrast to loperamide, verapamil and epinastine. The lower pKa value of ketotifen compared to the other compounds suggests the importance of a positive charge to electrostatically interact with the polar groups of phospholipids and enable membrane insertion [38,39]. Next, cellular uptake of Cy5-mRNA in HeLa cells was quantified for the respective CADosomes, showing >90% Cy5-positive cells independent of the production method and CAD type (Fig. 3B–C). Interestingly, only desipramine (DSI)-DOPE showed comparable mRNA internalization efficiency to NT-DOPE, outperforming their CADosome counterparts with amitriptyline and imipramine, only differing in the substitution degree of the amine group. This trend was also reflected in the eGFP expression, with only DSI-DOPE showing similar mRNA delivery efficiency to NT-DOPE, reaching up to 90% eGFP+ cells with high expression levels (Fig. 3D–E). Also CADosomes based on DES, with a secondary amine concealed in a more bulky piperazine ring structure, significantly underperformed. These data altogether indicate that tricyclic, lipid-like CADs with a segregated secondary amine group are preferred both for CADosome formation and cytosolic mRNA delivery [37]. However, a more detailed structure-activity relationship would be required to verify this hypothesis.

2.4. Evaluation of the pharmacological activity of CADosomes using Nanoluciferase Binary Technology (NanoBIT®)

CADosomes that are able to deliver both a functional CAD and therapeutic mRNA in one single NP formulation would provide ample opportunities for combination therapy. To assess if CADs remain pharmacologically active after incorporation in CADosomes, a previously described luminescence bioassay was used, based on HEK293T (Human Embryonic Kidney) cells stably expressing the 5-HT_{2A}R (serotonin 2A receptor) and the cytosolic protein β -arrestin 2 (β arr2) in the Nanoluciferase Binary Technology (NanoBIT®) system (Fig. 4A) [54–57]. Binding of a 5-HT_{2A}R receptor agonist, in this case lysergic acid diethylamide (LSD), results in β arr2 recruitment to the 5-HT_{2A}R and the concomitant functional complementation of the luciferase enzyme, which can be monitored through the luminescence generated in the presence of the substrate. *Vice versa*, binding of an antagonist to the 5-HT_{2A}R, *e.g.* nortriptyline (NT), will hamper agonist-induced β arr2 recruitment and the formation of a luminescence signal. As expected, increasing concentrations of free NT (30 μ M and 100 μ M), reduced or even completely prevented 5-HT_{2A}R activation by 1 μ M, respectively 10 nM, of the agonist LSD (Fig. 4B). Furthermore, independent of the production method, transfecting the HEK293T cells with NT-DOPE CADosomes impaired LSD-induced 5-HT_{2A}R activation with increasing N/P ratio, corresponding with a higher CAD content. Remarkably, no



(caption on next page)

Fig. 2. Evaluating nortriptyline (NT)-DOPE CADosomes for cytosolic delivery of eGFP-encoding mRNA in a HeLa cell line. **(A–B)** Evaluation of cellular uptake of NT-DOPE CADosomes with different N/P ratios, loaded with Cy5-labeled mRNA, in HeLa cells as analyzed via flow cytometry and expressed as Cy5+ cells and Cy5 relative mean fluorescence intensity (rMFI Cy5; normalized to non-treated control (NTC)), respectively. **(C)** Representative confocal images of HeLa cells after transfection with Cy5-mRNA NT-DOPE CADosomes N/P 9, with nuclei (blue) and intracellular Cy5-mRNA (magenta). Scale bars correspond to 100 μ m. **(D–E)** eGFP expression 24 h after transfection with NT-DOPE CADosomes N/P 3, 6, 9 and 12, DOTAP-DOPE N/P 2 and negative controls (CTRL) complexing luciferase-encoding mRNA, expressed as percentage eGFP+ HeLa cells and eGFP rMFI, respectively. **(F)** Transfection yield (i.e. eGFP expression normalized to intracellular mRNA dose) of NT-DOPE CADosomes N/P 9 compared to DOTAP-DOPE lipoplexes. **(G)** Representative confocal images of HeLa cells 24 h after transfection with eGFP-mRNA NT-DOPE CADosomes N/P 9, with nuclei (blue) and enhanced green fluorescent protein (eGFP) expression (green). Scale bars correspond to 100 μ m. Data are represented as mean \pm the standard error of the mean (SEM) for three independent repeats ($n = 3$). Statistical analysis was performed using One Way Anova with Tukey Correction (ns $p > 0.05$, * $p \leq 0.05$, ** $p \leq 0.01$, *** $p \leq 0.001$, **** $p \leq 0.0001$). (For interpretation of the references to color in this figure legend, the reader is referred to the web version of this article.)

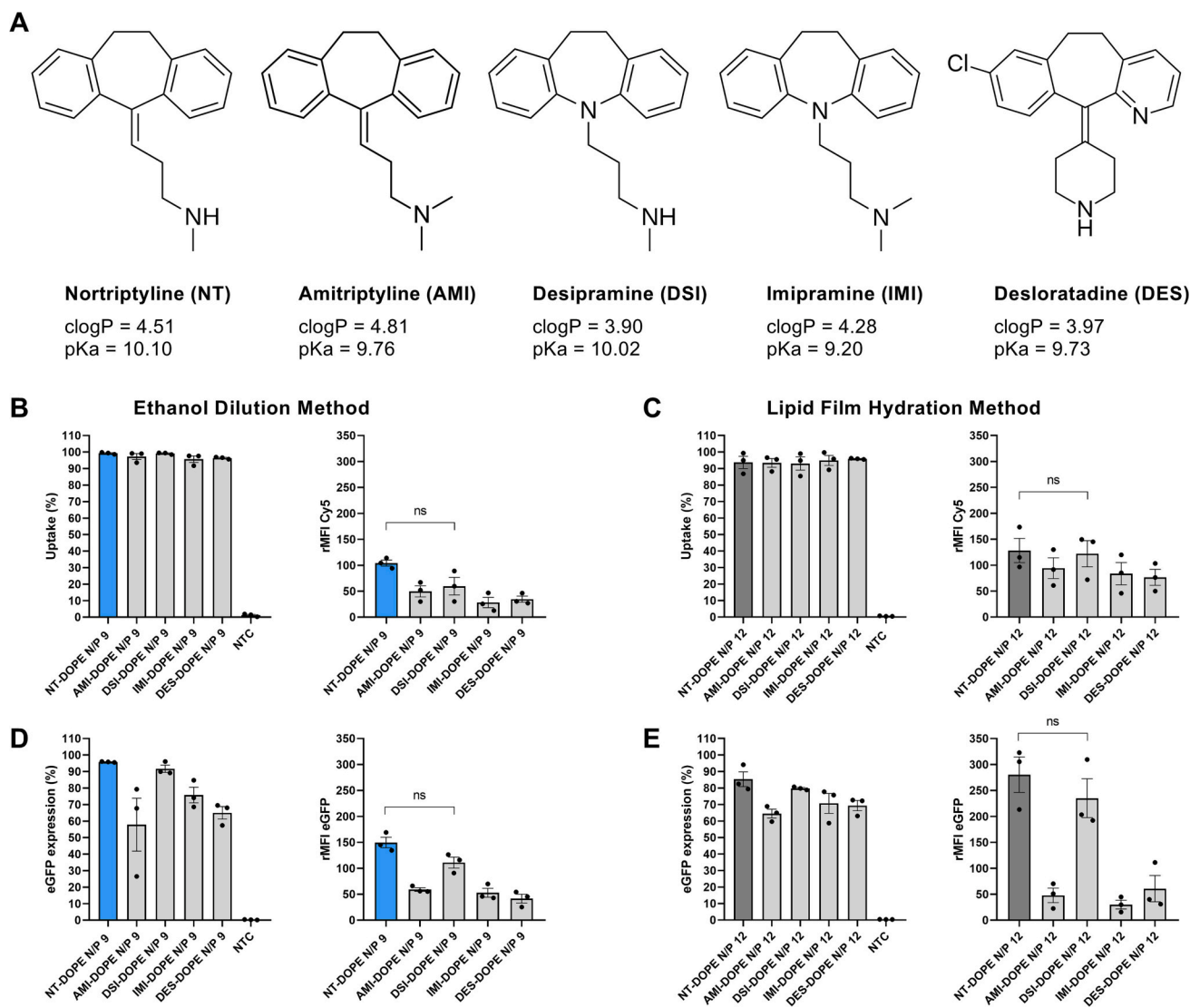


Fig. 3. Screening of different CADosomes for mRNA delivery in HeLa cells. **(A)** Molecular structure of CAD molecules which were capable of forming CADosomes in combination with DOPE (50:50 molar ratio). **(B–C)** Flow cytometry quantification of cellular uptake and **(D–E)** eGFP-mRNA expression of AMI-DOPE, DSI-DOPE, IMI-DOPE and DES-DOPE compared to NT-DOPE CADosomes, loaded with Cy5-labeled or eGFP-encoding mRNA, respectively. The latter CADosomes were prepared via ethanol dilution **(B–D)** and lipid film hydration method **(C–E)** using optimal N/P ratios. Data are represented as mean \pm the standard error of the mean (SEM) for three independent repeats ($n = 3$). Statistical analysis was performed using One Way Anova with Tukey Correction (ns $p > 0.05$). (rMFI = relative mean fluorescence intensity normalized to non-treated cells (NTC)).

significant difference could be observed in 5-HT_{2A}R antagonism between 30 μ M of free NT and NT-DOPE CADosomes N/P 9, which contain the equal antagonist concentration. The obtained real-time receptor activation profiles clearly indicate similar trends (Fig. 4C, D and E and Fig. S4A). Since it was clearly demonstrated in Fig. 1 that NT is integrated in the lipid vesicles, leading to a positive surface charge and

enabling mRNA complexation, these data suggest that the pharmacological activity of the TCA nortriptyline remains unaffected after CADosome incorporation.

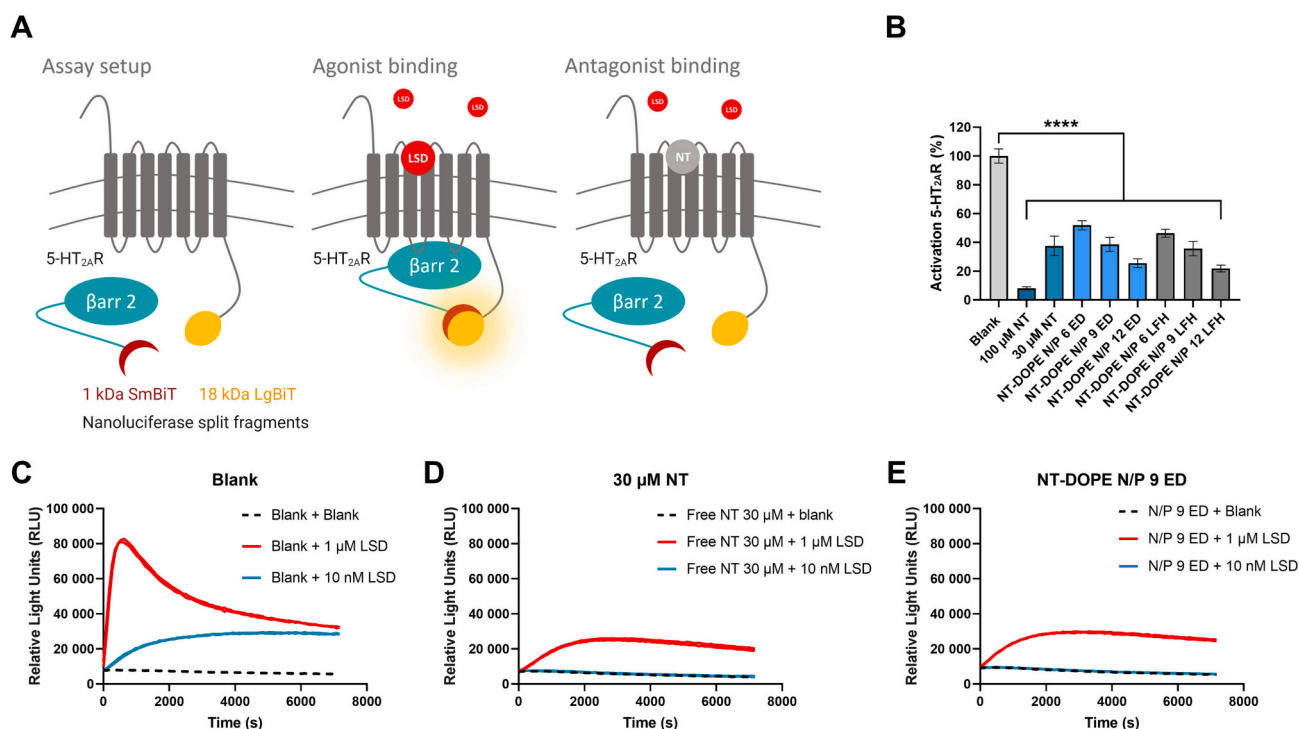


Fig. 4. Evaluation of the pharmacological activity of nortriptyline following CADosome formulation using a Nanoluciferase Binary Technology (NanoBiT®) bioassay (**A**) Schematic illustration of the NanoBiT® system, with HEK293T cells stably expressing two inactive luciferase split fragments (1 kDa SmBiT and 18 kDa LgBiT), coupled to the 5-HT_{2A}R (serotonin 2A receptor) and the cytosolic protein β-arrestin 2 (βarr2), respectively [54–56]. Binding of a receptor agonist, in this case LSD, results in βarr2 recruitment to the 5-HT_{2A}R with the concomitant functional complementation of the enzyme, which can be monitored through luminescence read-out. Binding of a receptor antagonist, e.g. nortriptyline (NT), inhibits LSD-induced βarr2 recruitment and subsequent luciferase complementation. (**B**) Percentage 5-HT_{2A}R activation induced by blank, free NT (30 and 100 μM) and different NT-DOPE CADosomes loaded with eGFP-mRNA, measured by calculating the normalized area under the curve (AUC) values of the receptor activation profiles. 1 μM LSD was added to all samples and luminescence was continuously monitored for 2 h. Data are represented as mean ± the standard error of the mean (SEM) for three independent repeats ($n = 3$). Statistical analysis was performed using One Way Anova with Tukey Correction (**** $p \leq 0.0001$). (**C–E**) One representative activation profile of blank, free NT 30 μM and mRNA NT-DOPE N/P 9, respectively.

2.5. CADosome-mediated Cre-recombinase mRNA delivery

Next, a HeLa reporter cell line stably expressing the Cre reporter plasmid pLV-CMV-LoxP-DsRed-LoxP-eGFP was used to further demonstrate the delivery efficiency of CADosomes as nanocarriers of Cre-recombinase-encoding mRNA [58]. Cre-recombinase is a tyrosine recombinase enzyme that is able to excise the DsRed stop-codon between loxP sites, causing a shift from red (DsRed+) to green (eGFP+) fluorescence in the reporter cells (Fig. 5A) [58–60]. Both NT-DOPE CADosomes N/P 9 and N/P 12 reached up to 80% eGFP+ cells 24 h post-transfection, as measured via flow cytometry. Interestingly, equal recombination efficiency was obtained as with cationic DOTAP-DOPE lipoplexes (Fig. 5B). A clear cell population shift could be observed on representative dot-plots of CADosomes N/P 9 (82.6% eGFP+ cells) and DOTAP-DOPE N/P 2 (79.4% eGFP+ cells) compared to non-treated cells (NTC) (Fig. 5C). These data indicate the versatility of CADosomes to deliver functional mRNA cargo's in a highly effective manner in line with conventional cationic lipoplexes.

2.6. CADosome-mediated mRNA delivery in hard-to-transfect primary bovine corneal epithelial cells

Having established that NT-DOPE CADosomes are able to deliver mRNA in HeLa cells, we next sought to evaluate their delivery performance in a more difficult-to-transfect primary cell type. As Fig. 1 indicated that at least a fraction of the mRNA will likely be exposed at the surface of the particles, we first further optimized our transfection protocol to reduce the risk of mRNA degradation during transfection. Raes et al. recently demonstrated that an additional washing step with

OptiMEM before adding mRNA to the cells allowed to remove degradative enzymes from the culture medium and improved transfection efficiency with a physical delivery method [61]. Applying this protocol to CADosomes, the eGFP expression likewise increased almost two-fold in HeLa cells, outperforming the transfection efficiency of DOTAP-DOPE lipoplexes (Fig. S5 A–D). Next, freshly excised bovine eyes were collected at a local slaughterhouse and the corneal epithelial layer was separated from corneal stroma (Fig. 6A). The obtained primary bovine corneal epithelial cells (PBCECs) were cultured and subsequently treated with NT-DOPE CADosomes, loaded with a Cy5-labeled or eGFP-encoding mRNA. Despite 80% of the PBCECs demonstrating successful mRNA internalization following NT-DOPE transfection, the extent of cellular uptake was ~10-fold lower compared to the cationic DOTAP-DOPE lipoplexes (Fig. 6B). Again, the difference in surface charge between both complexes could be responsible for this observation. Surprisingly, even with strongly reduced cellular internalization, the resulting eGFP expression 24 h post-transfection was highest for NT-DOPE CADosomes, reaching almost 55% eGFP positive PBCECs with >30% higher eGFP expression than the DOTAP:DOPE positive control (Fig. 6C–E). Of note, taking into account the lower cellular uptake of mRNA obtained via transfection with NT-DOPE CADosomes N/P 12, a ten-fold higher mRNA transfection yield was reached relative to the DOTAP-DOPE lipoplexes (Fig. 6D). Furthermore, treatment with CADosomes at higher N/P ratio did not affect PBCEC cell viability in contrast to previously described experiments in HeLa cells (Fig. S3B). As illustrated via representative flow cytometry dot-plots (Fig. 6E), a significant cell population shift was observed for NT-DOPE N/P 9 compared to NTC, indicating a high transfection efficiency. Notably, in this hard-to-transfect cell type CADosomes NT-DOPE N/P 9 and N/P 12

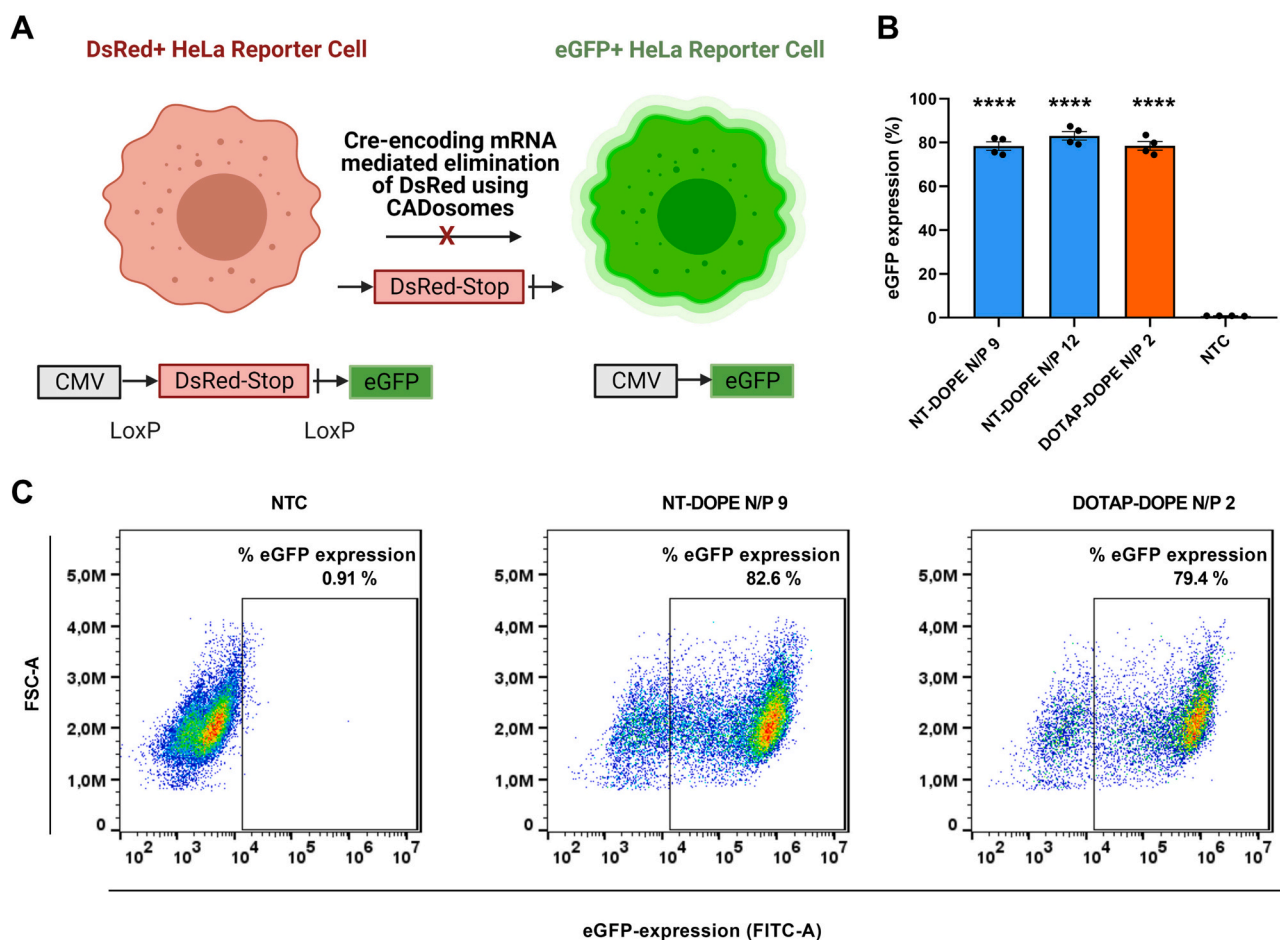


Fig. 5. CADosome-mediated delivery of Cre-recombinase encoding mRNA (Cre-mRNA) in a HeLa reporter cell line. (A) Schematic illustration of HeLa reporter cells shifting from DsRed+ to eGFP+ after Cre-recombinase mediated elimination of the DsRed stop-codon following successful delivery of Cre-encoding mRNA via CADosomes. Created with BioRender.com (B) Percentage eGFP+ cells as analyzed via flow cytometry 24 h after transfection with NT-DOPE CADosomes N/P 9–12 and DOTAP-DOPE N/P 2. Data are represented as mean \pm the standard error of the mean (SEM) for minimum three independent repeats ($n \geq 3$). Statistical analysis was performed using One Way Anova with Tukey Correction (**** $p \leq 0.0001$). (C) Representative flow cytometry dot-plots of non-treated cells (NTC) and NT-DOPE CADosomes N/P 9 or DOTAP-DOPE N/P 2 transfected HeLa reporter cells, respectively.

markedly outperformed state-of-the-art ionizable lipid MC3-LNPs, reaching >90% eGFP+ cells while only about half of the cells were transfected with LNPs. In addition, CADosomes demonstrated >20-fold higher eGFP expression levels (Fig. S6A–E). Such high expression levels also exceed what was reported in Fig. 6C, which could be explained by donor variability in the PBCECs, which were now obtained from another bovine eye. The abovementioned data proposes CADosomes as a suitable carrier for mRNA delivery in human *ex vivo* explant models or for *in vivo* application to the cornea.

2.7. *In vivo* mRNA delivery by CADosomes to the cornea of rabbits

Given the high mRNA delivery efficiency of CADosomes in PBCECs, we next aimed to investigate mRNA delivery in an *in vivo* rabbit eye model [62–64]. Many ophthalmic diseases, such as trauma and dry eyes, are due to malfunctions at the level of the cornea, leading to severe visual impairment. Often, corneal transplantation is the only therapeutic option for these patients to improve quality of life [65]. Nucleic acid therapeutics could offer new therapeutic opportunities for corneal repair, albeit that their functional delivery to the corneal epithelium remains challenging. To evaluate the potential of CADosomes for *in vivo* mRNA delivery to the cornea, a total of 9 New Zealand white rabbits were divided in 3 groups and the corneal surface was treated for 4 h with eye drops containing (a) PBS as negative control, (b) free mRNA, or (c) eGFP-mRNA NT-DOPE N/P 9 CADosomes at a total mRNA concentration

of 2 $\mu\text{g}/\text{mL}$. Up to 48 h post administration, clear eGFP expression could be visualized in specific areas of the cornea after exposure to CADosomes (Fig. 7A). In contrast, both eyes treated with only PBS or free mRNA did not contain such regions of high eGFP fluorescence, as measured via fluorescence photography (Fig. S7). Furthermore, the thickness of the cornea and epithelial tissue were determined via Optical Coherence Tomography (OCT) and H&E imaging. No significant difference was observed between all treatment conditions (Fig. 7B–C and Fig. S8A). Both histological analysis (Fig. 7D) and a Terminal deoxynucleotidyl transferase dUTP Nick End Labeling (TUNEL) assay (Fig. S8B) indicated that tissue morphology remained intact [62]. To conclude, this proof-of-concept *in vivo* data showed the potential of mRNA CADosomes for local nucleic acid delivery towards the cornea.

3. Conclusion

Lipid nanoparticle (LNP) formulations have greatly facilitated the recent clinical translation of RNA therapeutics, but current compositions still suffer from relatively low intracellular delivery efficiency and safety concerns, especially for repeated administration. In addition, to enable drug combination therapies with a single LNP, strategies to co-encapsulate small molecule drugs are highly sought after. Here, we have discovered that tricyclic cationic amphiphilic drugs (CADs) can be repurposed as structural components of lipid-based nanoparticles (termed CADosomes) for mRNA delivery in combination with the

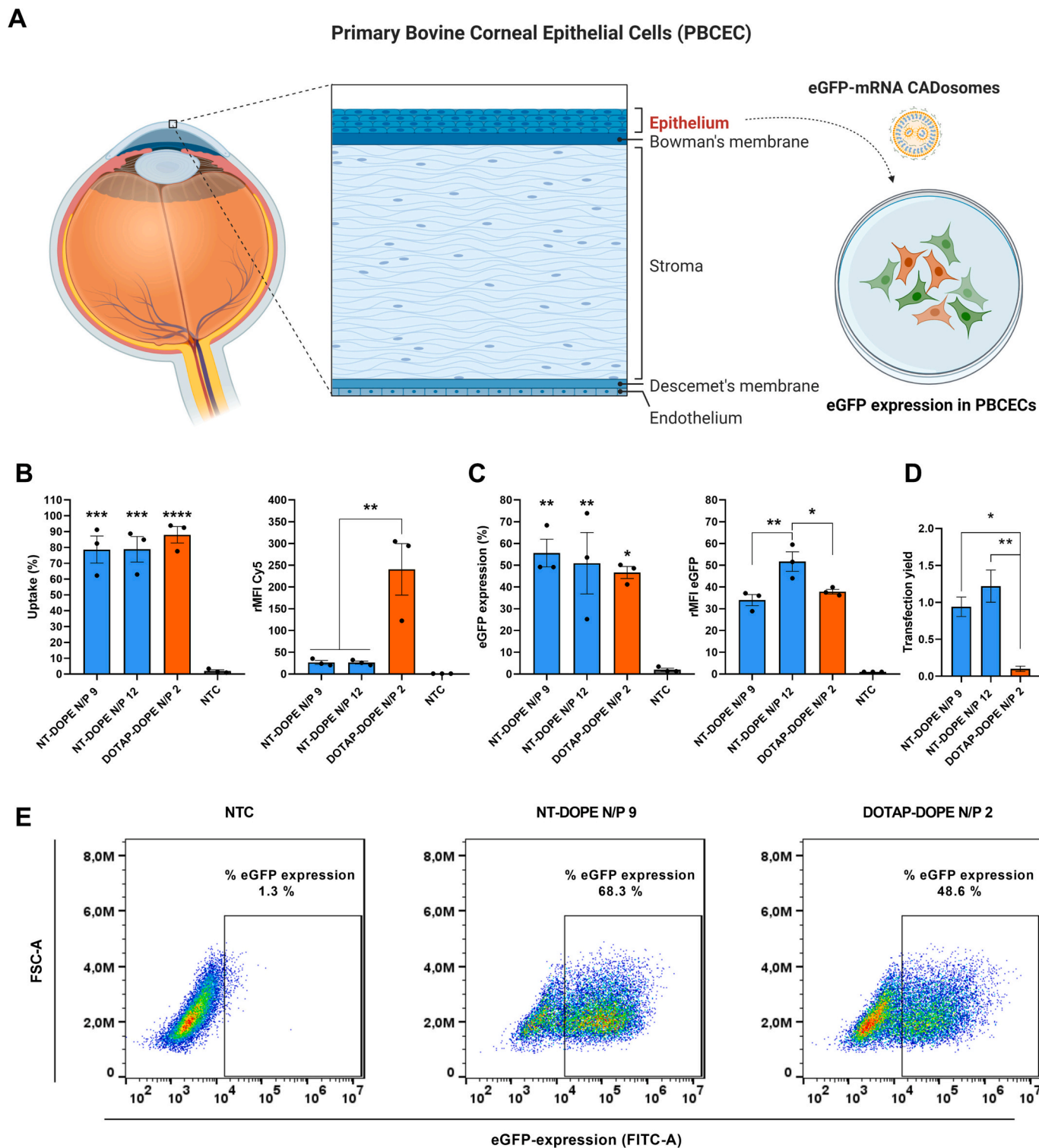


Fig. 6. Delivery of mRNA with NT-DOPE CADosomes in primary bovine corneal epithelial cells (PBCEC). (A) Schematic illustration of the different tissue layers in the human cornea. The corneal epithelial layer was separated from corneal stroma using stainless tweezers and cultured for mRNA transfection. Created with BioRender.com (B) Cell uptake of Cy5-mRNA via NT-DOPE CADosomes N/P 9–12 was significantly lower compared to cationic DOTAP-DOPE lipoplexes after 4 h incubation. (C–D) CADosomes outperformed DOTAP-DOPE lipoplexes, reaching a ten-fold higher transfection yield for delivery of eGFP-mRNA to hard-to-transfect PBCECs, as measured 24 h after administration. (E) Representative dot-plots of non-treated cells (NTC), eGFP-mRNA NT-DOPE CADosomes N/P 9 and eGFP-mRNA DOTAP-DOPE N/P 2 lipoplexes analyzed via flow cytometry. Data are represented as mean \pm the standard error of the mean (SEM) for three independent repeats ($n = 3$). Statistical analysis was performed using One Way Anova with Tukey Correction (* $p \leq 0.05$, ** $p \leq 0.01$, *** $p \leq 0.001$, **** $p \leq 0.0001$).

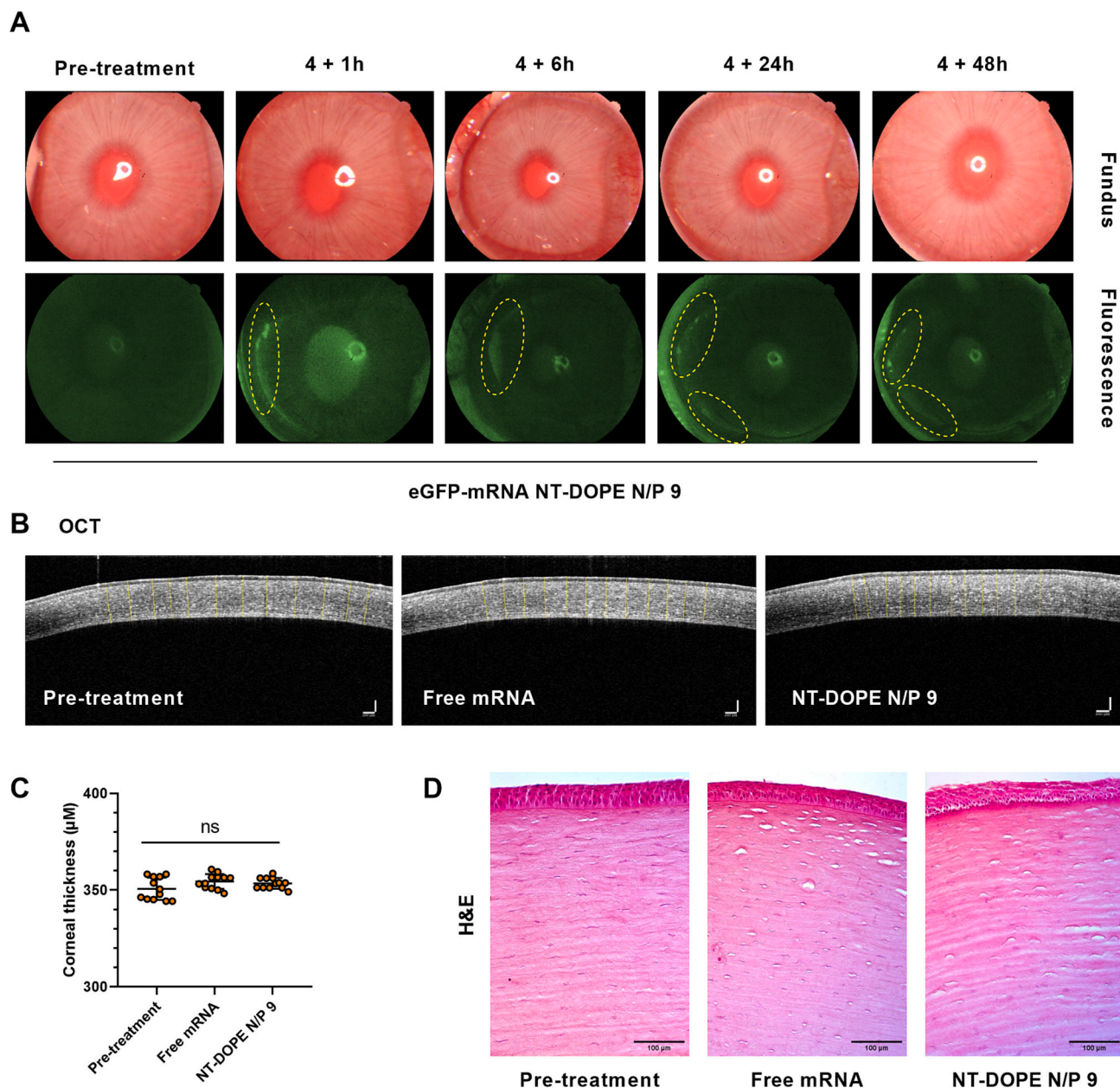


Fig. 7. *In vivo* evaluation of eGFP-mRNA delivery and corneal toxicity of mRNA CADosomes in a rabbit model. (A) Color fundus and fluorescence images of rabbit eyes treated with eGFP-mRNA NT-DOPE N/P 9 CADosomes at a final concentration of 2 $\mu\text{g}/\text{mL}$. The marked yellow circles indicate regions with high eGFP expression at different timepoints post treatment. (B–C) 2D Optical Coherence Tomography (OCT) images visualizing the corneal thickness pre- and post-administration. No significant change could be observed ($n = 12$ measurements at different locations of the cornea, analyzed via ImageJ software). Scale bars correspond to 100 μm . Statistical analysis was performed using One Way Anova with Tukey Correction (ns $p \geq 0.05$). (D) Histology of the corneal surface treated with free eGFP-mRNA and eGFP-mRNA CADosomes, respectively. The presented images are representative of three rabbits for each group ($n = 3$). (For interpretation of the references to color in this figure legend, the reader is referred to the web version of this article.)

fusogenic helper lipid DOPE, thereby successfully replacing conventional cationic or ionizable lipids. Owing to the particular physico-chemical properties of CADs, no prior derivatization with additional hydrophobic moieties is required. Efficient mRNA delivery (encoding for eGFP or Cre-recombinase) was achieved in a HeLa epithelial adenocarcinoma cell line as well as hard-to-transfect primary bovine corneal epithelial cells. Moreover, using a NanoBIT® bioassay, we demonstrated that a model tricyclic CAD (*in casu* the tricyclic antidepressant nortriptyline) could maintain its pharmacological activity after CADosome incorporation. Finally, *in vivo* mRNA delivery to the corneal epithelium and toxicity studies in a rabbit model indicated the potential of mRNA CADosomes for future ophthalmic applications. Therefore, we

propose CADosomes as a versatile technology for co-delivery of CADs and RNA therapeutics, providing opportunities for drug combination therapy.

4. Materials and methods

4.1. Messenger RNA constructs

The 996 nucleotide long, CleanCap® Enhanced Green Fluorescent Protein Messenger RNA (eGFP-mRNA), modified with 5-methoxyuridine (5-moU), a Cyanine-5 labeled CleanCap® Enhanced Green Fluorescent Protein Messenger RNA (Cy5-mRNA), modified with 5-methoxyuridine

(5-moU) and a nucleoside-modified (5mC, Ψ) mRNA encoding firefly luciferase (fLuc-mRNA), were purchased from TriLink (San Diego, CA). Cre-recombinase mRNA (Cre-mRNA) was synthesized by the lab of Prof. Pieter Vader (Laboratory of Clinical Chemistry and Hematology, University Medical Center Utrecht, Utrecht, The Netherlands) [58,59]. The mRNA stocks were dissolved in nuclease-free water (Ambion®-Life Technologies, Ghent, Belgium) and stored in small aliquots at -80°C at a concentration of $1\ \mu\text{g}/\mu\text{L}$. The mRNA stock concentration was determined from absorption measurements at 260 nm with a NanoDrop 2000c UV-Vis spectrophotometer (Thermo Fisher Scientific, Rockford, USA).

4.2. Preparation of CAD-DOPE lipid vesicles

The cationic amphiphilic drugs (CADs) nortriptyline hydrochloride (NT), amitriptyline hydrochloride (AMI), desipramine hydrochloride (DSI), imipramine hydrochloride (IMI), ketotifen (KET), loperamide hydrochloride (LOP) and verapamil hydrochloride (VER) were purchased from Sigma-Aldrich (Overijse, Belgium) and desloratadine (DES) and epinastine hydrochloride (EP) from Cayman Chemical (Michigan, USA). The lipids DOTAP (1,2-dioleoyl-3-trimethylammonium-propane) and DOPE (1,2-dioleoyl-*sn*-glycero-3-phosphoethanolamine) were purchased from Avanti Polar Lipids (Alabaster, USA). Two literature-based methods were used to produce CAD-DOPE vesicles [45–47]. For the ethanol dilution (ED) method, CADs (10 mg/ml) and DOPE (25 mg/ml) were separately dissolved in absolute ethanol. CAD-DOPE vesicles (50:50 molar ratio) were prepared by transferring the appropriate amount of CADs and DOPE into a round-bottom flask, followed by dropwise addition of 4-(2-hydroxyethyl)-1-piperazineethanesulfonic acid (HEPES) buffer (pH 7.4, 20 mM) and tip-sonication ($6 \times 10\ \text{s}$, amplitude 10%; 10 s on/15 s off; Branson Digital Sonifier®, Danbury, USA). The final CAD-DOPE concentration after dilution in HEPES buffer (pH 7.4, 20 mM) was 3.56 mM. For the lipid film hydration method CAD (10 mg/ml) and DOPE (25 mg/ml) were dissolved in chloroform (50:50 molar ratio) and transferred to a brown glass vial, followed by chloroform evaporation under nitrogen flow. Next, the CAD-DOPE lipid film was rehydrated with HEPES buffer (pH 7.4, 20 mM), followed by tip-sonication and further dilution in HEPES buffer (pH 7.4, 20 mM) to obtain a final CAD-DOPE concentration of 3.56 mM. The classically used cationic DOTAP-DOPE liposomes (50:50 molar ratio) were likewise prepared via lipid film hydration, as previously reported in the literature [44,46] and diluted in HEPES buffer (pH 7.4, 20 mM) to obtain a final lipid concentration of 3.9 mM. Hydrodynamic diameter, polydispersity index (PDI) and zeta-potential of all formulations were determined via dynamic light scattering (DLS) (Zetasizer Nano, Malvern Instruments, Worcestershire, United Kingdom).

4.3. Physicochemical analysis of mRNA CADosome lipoplexes

To obtain stable mRNA CAD-DOPE complexes (further denoted as CADosomes) and DOTAP-DOPE mRNA lipoplexes, CAD-DOPE vesicles and DOTAP-DOPE liposomes were complexed with equal volumes of mRNA diluted in nuclease-free water (Ambion®-Life Technologies, Ghent, Belgium) for 10 min at room temperature, reaching the desired nitrogen-to-phosphate (N/P) ratio. Hydrodynamic diameter, polydispersity index (PDI) and zeta-potential of mRNA CADosomes and DOTAP-DOPE lipoplexes were determined via dynamic light scattering (DLS) (Zetasizer Nano, Malvern Instruments, Worcestershire, United Kingdom). Transmission electron microscopy (TEM) images of mRNA CADosomes were recorded at the VIB-UGent BioImaging Core facility with a transmission electron microscope JEM1400plus operating at 80 kV (JEOL, Tokyo, Japan). The samples were prepared by depositing a drop (15 μL) of mRNA CADosomes on a formvar/C-coated hexagonal copper grid (EMS G200H-Cu), followed by five repeated washing steps in double-distilled water and a final staining with uranyl-acetate. The samples were allowed to dry at room temperature. The complexation

efficiency of mRNA CADosomes was measured via Fluorescence Correlation Spectroscopy (FCS) as explained in detail in previous work to quantify the complexation of fluorescently labeled RNA nanocarriers [48]. Briefly, this microscopy-based technique monitors fluorescence intensity fluctuations of fluorescent molecules diffusing in and out of the fixed excitation volume of a confocal microscope. Fluorescence time traces (60s) were recorded by focusing a 640 nm laser line through a water immersion objective lens ($60\times$ Plan Apo VC, NA 1.2, Nikon, Japan) of a confocal microscope (Nikon C2, Japan) at about 50 μm above the bottom of a glass-bottom 96-well plate (Greiner Bio-one, Frickenhausen, Germany), which contained 50 μL Cy5-mRNA CADosomes, uncomplexed Cy5-mRNA or blank HEPES buffer (pH 7.4, 20 mM), respectively. The fluorescence signal was recorded by a photon counting instrument (Pico-Harp 300, PicoQuant, Berlin, Germany) equipped with MATLAB software (MathWorks, USA).

4.4. Cell lines and culture conditions

The human cervical epithelial adenocarcinoma HeLa cell line was obtained from American Type Culture Collection (ATCC, Manassas, USA). A DsRed+ HeLa reporter cell line, stably expressing the fluorescent Cre-recombinase reporter plasmid (pLV-CMV-LoxP-DsRed-LoxP-eGFP), was used as previously reported [58–60]. HeLa cells were cultured in Dulbecco's Modified Eagle Medium: Nutrient F-12 (DMEM/F-12) (Gibco®-Life Technologies, Grand Island, NY, USA), supplemented with 10% fetal bovine serum (FBS, Hyclone™, GE Healthcare, Machelen, Belgium), 2 mM L-Glutamine and 100 U/mL penicillin/streptomycin (hereafter collectively called 'complete cell culture medium' or CCM). The development of a Human Embryonic Kidney cell line (HEK293T), stably expressing the 5-HT_{2A}R (Serotonin 2A Receptor) and the cytosolic protein β -arrestin 2 (β arr2) in the NanoBiT® system was previously reported [54–56]. To obtain primary bovine corneal epithelial cells (PBCECs), freshly excised bovine eyes were collected at a local slaughterhouse (Flanders Meat Group, Zele, Belgium) and were transferred within 30 min in cold CO₂-independent medium. The eyes were cleaned of excess tissue and then disinfected by dipping into a 5% ethanol solution. A trephine blade was used to collect 10 mm diameter corneal buttons. The corneal buttons were rinsed with DMEM (Gibco®-Life Technologies, Grand Island, NY, USA) containing antibiotics and divided in 4 equal parts using a scalpel, rinsed again with DMEM and placed in a 15 mg/ml Dispase II solution at 37 $^{\circ}\text{C}$ for 15–30 min. Hereafter the tissues were rinsed with PBS and the epithelial layer was separated from the corneal stroma using stainless tweezers. The obtained epithelial sheets are placed in separate wells with fresh DMEM containing antibiotics, 4.5 g/L D-glucose and 10% FBS. Once 80% confluency was reached in the wells, the epithelial tissue layer was removed and the PBCECs were transferred to cell culture flasks. All cell lines were cultured in a humidified atmosphere containing 5% CO₂ at 37 $^{\circ}\text{C}$ and culture medium was renewed every other day unless the 80% confluence level was reached.

4.5. Quantification of cellular internalization in HeLa by flow cytometry

To quantify the cellular internalization of mRNA via flow cytometry, HeLa cells were seeded in a 96-well plate (VWR® International, PA, USA) at a density of 10,000 cells/well (100 μL /well) and left to settle overnight. After dilution in OptiMEM®, the cells were transfected with Cy5-labeled mRNA CADosomes, fLuc-mRNA control CADosomes or Cy5-labeled mRNA DOTAP-DOPE lipoplexes (100 ng mRNA/well) during 4 h at 37 $^{\circ}\text{C}$ in humidified atmosphere containing 5% CO₂. Following incubation, the cells were washed with PBS and harvested by trypsinization (trypsin/EDTA 0.25%). After neutralization in CCM, the cell suspensions were transferred to a U-bottom 96-well plate (Greiner Bio-One GmbH, Vilvoorde, Belgium), which was centrifuged during 5 min at 500 g. Next, the cells were resuspended in 80 μL of flow buffer (PBS supplemented with 1% bovine serum albumin and 0.1% sodium azide)

and kept on ice until flow cytometry analysis. The samples were analyzed using the CytoFLEX® flow cytometer (Beckman Coulter, Krefeld, Germany) and CytoExpert software. Data analysis was performed using the FlowJo™ analysis software (Version 10.5.3, Treestar, Costa Mesa, CA, USA). The Mean Fluorescence intensity (MFI) of the tested mRNA formulations was normalized to a non-treated cell population (NTC) to calculate relative-Mean Fluorescence intensity (rMFI) values.

4.6. Quantification of eGFP-mRNA expression in HeLa by flow cytometry

To quantify the expression of eGFP-mRNA via flow cytometry, HeLa cells were seeded in a 96-well plate (VWR® International, PA, USA) at a density of 10.000 cells/well (100 µL/well) and left to settle overnight. After dilution in OptiMEM®, the cells were transfected with eGFP-mRNA CADosomes, fLuc-mRNA control CADosomes or eGFP-mRNA DOTAP-DOPE lipoplexes (100 ng mRNA/well) during 4 h at 37 °C in humidified atmosphere containing 5% CO₂. Following incubation, the cells were washed with PBS and incubated with fresh CCM for 24 h. Next, flow cytometry sample preparation data acquisition and analysis was performed as previously described. Transfection yield was calculated based on the following equation: (rMFI eGFP * eGFP expression %)/(rMFI Cy5 * Uptake %).

4.7. Visualization of cellular internalization and eGFP-expression in HeLa by confocal microscopy

HeLa cells were seeded in two separate black, cyclic olefin copolymer 96-well plates for high content imaging (PerkinElmer Health Sciences, Groningen, Nederland) at a density of 10.000 cells/well (100 µL/well) and left to settle overnight. To visualize Cy5-mRNA cytosolic internalization, Cy5-mRNA CADosomes (NT-DOPE) were added to the cells in OptiMEM® (100 ng Cy5-mRNA/well). Similar steps were performed to visualize eGFP expression using eGFP-mRNA CADosomes (100 ng eGFP/well). The cells were incubated for 4 h at 37 °C in humidified atmosphere containing 5% CO₂. Following incubation, the cells transfected with eGFP-mRNA CADosomes were washed with PBS and incubated with fresh CCM for 24 h until imaging, while the cells transfected with Cy5-mRNA CADosomes were fixed with 4% paraformaldehyde during 10–15 min at room temperature. Next, the nuclei were stained by adding one drop of VECTASHIELD® antifade mounting medium with DAPI per well (Vector Laboratories, CA, USA). The same procedure was applied on the cells containing eGFP-mRNA CADosomes after 24 h incubation. A laser scanning confocal microscopy (Nikon A1R HD confocal, Nikon, Japan), equipped with a 20× air objective lens (20× CFI Plan Apo VC, NA 0.75, WD 1000 µm, Nikon, Japan), with a laser box (LU-N4 LASER UNIT 405/488/561/640, Nikon Benelux, Brussels Belgium) and detector box (A1-DUG-2 GaAsP Multi Detector Unit, GaAsP PMT for 488 and 561 and Multi-Alkali PMT for 640 and 405 nm). The 405 nm, 488 nm and 640 nm laser were applied to excite the DAPI labeled nuclei, the eGFP protein and the Cy5-mRNA respectively. Fluorescence emission was detected through a 450/50 nm (MHE57010), 525/50 nm (MHE57030) and 700/75 nm (MHE57070) filter cube, respectively. A Galvano scanner was used for unidirectional scanning to acquire the channels sequential without line averaging and a scan speed of 0.042 FPS. The pinhole was set to 17.88 µm and the pixel size was 150 nm/pixel. NIS Elements software (Nikon, Japan) was applied for imaging.

4.8. Quantifying pharmacological activity of mRNA NT-DOPE CADosomes via a HEK293T cell Nanoluciferase Binary Technology (NanoBiT®) assay

To evaluate the pharmacological activity of the encapsulated norriptyline (NT) in mRNA CADosomes, a previously described HEK293T (Human Embryonic Kidney) reporter cell line was used, stably expressing the 5-HT_{2A}R (Serotonin 2A Receptor) and the cytosolic protein β-arrestin 2 (βarr2) in the NanoLuciferase Binary Technology

(NanoBiT®) system [54–57]. The latter consists of two (inactive) split fragments of the NanoLuc enzyme (1 kDa SmBiT and 18 kDa LgBiT), each fused to one of the potentially interacting proteins (5-HT_{2A}R and βarr2). Binding of a receptor agonist, in this case LSD, results in βarr2 recruitment to the 5-HT_{2A}R with the concomitant functional complementation of the enzyme, which can be monitored through the luminescence generated in the presence of the substrate [55]. The HEK293T cells were seeded in poly-D-lysine (Sigma-Aldrich, Overijse, Belgium) coated 96-well plates at a density of 50.000 cells/well (100 µL/well) and left to settle overnight. Next, the cells are rinsed with HBSS (Gibco®-Life Technologies, Grand Island, NY, USA) to remove remaining medium and serum, and 100 µL of the test solutions, containing mRNA CADosomes, free NT dissolved in HBSS (30 µM and 100 µM) or blank HBSS is placed on the cells, followed by another 4 h incubation in a humidified atmosphere at 37 °C and 5% CO₂. Subsequently, 25 µL of Nano-Glo® Live Cell Substrate (Promega, Madison, USA, diluted 1/20 in Nano-Glo® LCS Dilution Buffer, according to the manufacturer's protocol), is added to each well and the 96-well plate is transferred to a Tristar2 LB 942 multimode microplate reader (Berthold Technologies GmbH & Co, Germany). Upon stabilization of the luminescence signal, either concentrated LSD solution (Sigma-Aldrich, Overijse, Belgium) or the appropriate solvent controls are added, and the luminescence is continuously monitored for 2 h. The obtained real-time activation profiles are corrected for inter-well variability, followed by a calculation of the Area Under the Curve (AUC), from which the appropriate solvent control is deducted, as described in more detail in previous work [56].

4.9. Quantification of cellular Cy5-labeled mRNA internalization and eGFP-expression in primary bovine corneal epithelial cells (PBCECs) by flow cytometry

To quantify the gene expression of eGFP-mRNA and Cy5-mRNA cellular uptake via flow cytometry, PBCECs were seeded in a 96-well plate (VWR® International, PA, USA) at a density of 25.000 cells/well (100 µL/well) and left to settle overnight. Next, the cells were washed with OptiMEM® before adding eGFP-mRNA or Cy5-labeled mRNA CADosomes and DOTAP-DOPE lipoplexes diluted in OptiMEM® (100 ng mRNA/well), during 4 h at 37 °C in humidified atmosphere containing 5% CO₂. Following incubation, the cells were washed with PBS and incubated with fresh CCM for 24 h. The cells were then prepared for flow cytometry analysis as described above for the quantification of eGFP expression and Cy5-mRNA cellular internalization in HeLa cells.

4.10. Cell viability

HeLa cells (10.000 cells/well) and PBCECs (25.000 cells/well) were seeded in a 96-well plate and transfected with mRNA CADosome or DOTAP-DOPE lipoplexes. The cell viability was determined with the CellTiter-Glo® assay (Promega, Belgium). The culture plates and reconstituted assay buffer were placed at room temperature for 30 min, before initiating the assay. Subsequently, the CCM was replaced by 100 µL fresh CCM and an equal amount of assay buffer was added. To induce complete cell lysis, the plates were shaken during 2 min and the signal was allowed to stabilize the following 10 min. Next, 100 µL from each well was transferred to an opaque 96-well plate, which was measured with a GloMax® 96 Microplate Luminometer (Promega, Belgium).

4.11. Delivery of Cre-recombinase-mRNA in HeLa reporter cells by flow cytometry

To quantify eGFP expression after Cre-recombinase mediated elimination of the DsRed stop-codon, HeLa reporter cells were seeded in a 96-well plate (VWR® International, PA, USA) at a density of 10.000 cells/well (100 µL/well) and left to settle overnight. Next, the cells were washed with OptiMEM® before adding eGFP-mRNA CADosomes and DOTAP-DOPE lipoplexes diluted in OptiMEM® (100 ng mRNA/well),

during 4 h at 37 °C in humidified atmosphere containing 5% CO₂. Following incubation, the cells were washed with PBS and incubated with fresh CCM for 24 h. The cells were then prepared for flow cytometry analysis as described above for the quantification of eGFP expression in HeLa cells.

4.12. *In vivo* rabbit study

All animal experiments were performed under the guidelines of the Association for Research in Vision and Ophthalmology (ARVO). Experimental protocols were approved by the Institutional Animal Care and Use Committee (IACUC) of the University of Michigan (Protocol PRO00010388, PI Paulus). 1% tropicamide ophthalmic and 2.5% phenylephrine hydrochloride ophthalmic was used to dilate the rabbit pupils. A dose of ketamine (40 mg kg⁻¹; 100 mg/ml; Ketalar; Par Pharmaceutical) and xylazine (5 mg kg⁻¹, 100 mg/ml; Anased; MWI Veterinary Supply; VetOne; Boise) were intramuscularly injected to anesthetize the rabbits. A drop of 0.5% topical proparacaine (Alcaine; Alcon) was applied to the cornea for topical anesthesia. The rabbit's vitals such as heart rate, respiration rate, and body temperature were recorded and documented every 15 min using a pulse oximeter (Smiths Medical, USA). To maintain body temperature during the experiment and recovery time, the animals were placed on top of a water-circulating blanket (TP-700; Stryker Corporation) with an underpad (Medline, USA). Ophthalmic examination was conducted pre- and post-treatment up to 48 h, using a Zeiss A SL 130 slit lamp (Carl Zeiss Meditec, Jena, Germany). Several ocular structures such as the eyelids, cornea, conjunctiva, iris, anterior chamber, and lens were carefully examined and evaluated. At 48 h post-treatment, all animals were euthanized by intravenous injection of a euthanasia solution (0.22 mg kg⁻¹; Beuthanasia-D Special; Intervet) through the marginal ear vein. The eye tissues were collected for histological analysis.

4.13. *In vivo* eGFP-mRNA delivery into corneal epithelial cells

A total of 9 New Zealand white rabbits (both genders, males and females; weight from 2.4 to 3.2 kg; 3–5 months old) were used for *in vivo* eGFP-mRNA delivery. The rabbits were divided into 3 groups: (i) negative control group (cornea treated with PBS), (ii) cornea treated using eGFP-mRNA without CADosomes, and (iii) cornea treated by eGFP-mRNA CADosomes. 1 mL of PBS, free eGFP-mRNA and eGFP-mRNA CADosomes at final concentration of 2 µg/mL were applied on the surface of the cornea. The solution was administered dropwise up to 4 h, until the full dose had been given. At 1 h post-administration, the color fundus, fluorescence, and OCT images were acquired and followed for 48 h. The corneal thickness and epithelial thickness were determined using 2D OCT and H&E images. Color and fluorescent images of the cornea were obtained using a 50° Topcon color photography system (Topcon 50EX; Topcon Corporation). Photographs of the cornea were imaged by a Canon EOS-5D (Canon, Tokyo, Japan). OCT evaluation was done using a spectral domain Ganymede-II-HR OCT imaging system with modification (Ganymede-II-HR; Thorlabs, Germany), as explained in detail in the following references[64,66].

4.14. *In vivo* biosafety analysis

Histological analysis and Terminal deoxynucleotidyl transferase dUTP Nick End Labeling (TUNEL) assay were carried out to examine the structure of the cornea after treatment. Treated rabbits were euthanized at 48 h post treatment. The eyeballs were isolated and injected with 100 µL of 10% formalin. The harvested tissues were pre-fixed in Davidson fixation solution at room temperature for 24 h. The samples were transferred to 50% ethanol solution and incubated for 8 h. Next, the samples were placed in 70% ethanol solution for 24 h before embedding in paraffin. The tissues were sectioned to a thickness of 4 µm using a Leica Autostainer XL (Leica Biosystems) for H&E staining and TUNEL

assay analysis. The TUNEL assay was performed using the *in situ* cell death detection kit (Promega, USA) as previously reported [64]. The corneal morphology was evaluated along with the microstructural change of the treated tissue on the H&E images. All slides were images with a Leica DM600 light microscope (Leica Biosystems). Digital images were captured using a BF450C camera for H&E and a BF360C camera for TUNEL (DM600; Leica Biosystems).

4.15. Statistical analysis

All experiments were performed as technical triplicate and 3 independent biological repeats ($n = 3$) unless otherwise stated. All data are presented as mean ± standard error of the mean (SEM). Statistical analysis was performed using the 8th version of the GraphPad Prism software. One-way ANOVA with Tukey Correction was applied to compare multiple conditions, whereas the student *t*-test was used for direct comparison of 2 conditions. A *p* value ≤ 0.05 was considered *a priori* to be statistically significant (ns $p > 0.05$, * $p \leq 0.05$, ** $p \leq 0.01$, *** $p \leq 0.001$, **** $p \leq 0.0001$).

Author contributions

The manuscript was written through contributions of all authors. All authors have given approval to the final version of the manuscript.

CRediT authorship contribution statement

Bram Bogaert: Conceptualization, Methodology, Validation, Formal analysis, Investigation, Writing – original draft, Visualization. **Félix Sauvage:** Methodology, Writing – review & editing, Supervision. **Roberta Guagliardo:** Conceptualization, Methodology, Investigation, Writing – review & editing. **Cristina Muntean:** Conceptualization, Methodology, Investigation, Writing – review & editing. **Van Phuc Nguyen:** Methodology, Investigation, Writing – review & editing. **Eline Pottie:** Methodology, Investigation, Formal analysis, Writing – review & editing. **Mike Wels:** Methodology, Investigation, Writing – review & editing. **An-Katrien Minnaert:** Methodology, Investigation, Writing – review & editing. **Riet De Rycke:** Methodology, Investigation. **Qiangbing Yang:** Resources. **Dan Peer:** Resources, Supervision, Writing – review & editing. **Niek Sanders:** Methodology, Writing – review & editing. **Katrien Remaut:** Methodology, Resources, Writing – review & editing. **Yannis M. Paulus:** Methodology, Resources, Writing – review & editing. **Christophe Stove:** Methodology, Resources, Writing – review & editing. **Stefaan C. De Smedt:** Conceptualization, Supervision, Writing – review & editing. **Koen Raemdonck:** Conceptualization, Methodology, Validation, Formal analysis, Writing – original draft, Visualization, Supervision, Project administration, Funding acquisition.

Declaration of Competing Interest

The authors declare no competing financial interest.

Acknowledgments

B. Bogaert and A-K. Minnaert are doctoral fellows of the Research Foundation-Flanders (grant numbers 1S75019N, S28420N, FWO, Belgium). C. Muntean and K. Raemdonck additionally acknowledge the FWO for funding through research grant 3G039419. R. Guagliardo and M. Wels are doctoral fellows within the NANOMED project, which has received funding from the European Union's Horizon 2020 Research and Innovation Programme Marie Skłodowska Curie Innovative Training Networks (ITN) under grant number 676137. This project has additionally received funding from the European Research Council (ERC) under the European Union's Horizon 2020 research and innovation programme (Grant agreement No. 101002571). We acknowledge the donation of New Zealand White rabbits from the Center for Advanced

Models and Translational Sciences and Therapeutics (CAMTraST) at the University of Michigan. Y.M. Paulus acknowledges funding support from the NIH National Eye Institute (NEI) (award number 1K08EY027458) along with the Alcon Research Institute Young Investigator Grant and unrestricted departmental support from Research to Prevent Blindness. This work used the Vision Research Core Center funded by P30EY007003 from the NEI. The authors thank the Centre for Advanced Light Microscopy at Ghent University (Belgium) for the use and support of microscopy experiments, the Laboratory of Toxicology at Ghent University (Belgium) for the use of the NanoBiT® Assay and the Department of Ophthalmology and Visual Sciences at the University of Michigan for the collaboration on the *in vivo* rabbit model.

Appendix A. Supplementary data

Supplementary data to this article can be found online at <https://doi.org/10.1016/j.jconrel.2022.08.009>.

References

- R. Kanasty, J.R. Dorkin, A. Vegas, D. Anderson, Delivery materials for siRNA therapeutics, *Nat. Mater.* 12 (2013) 967–977.
- S. DeWeerd, RNA therapies explained, *Nature* 574 (2019) S2–S3.
- R.L. Setten, J.J. Rossi, S.P. Han, The current state and future directions of RNAi-based therapeutics, *Nat. Rev. Drug Discov.* 18 (2019) 421–446.
- U. Sahin, K. Karikó, Ö. Türeci, mRNA-based therapeutics—developing a new class of drugs, *Nat. Rev. Drug Discov.* 13 (2014) 759–780.
- N. Pardi, M.J. Hogan, F.W. Porter, D. Weissman, mRNA vaccines—a new era in vaccinology, *Nat. Rev. Drug Discov.* 17 (2018) 261–279.
- J. Kim, Y. Eyeris, M. Gupta, G. Sahay, Self-assembled mRNA vaccines, *Adv. Drug Deliv. Rev.* 170 (2021) 83–112.
- S.F. Dowdy, Overcoming cellular barriers for RNA therapeutics, *Nat. Biotechnol.* 35 (2017) 222–229.
- H. Zhang, K. Rombouts, L. Raes, R. Xiong, S.C. De Smedt, K. Braeckmans, K. Remaut, Fluorescence-based quantification of messenger RNA and plasmid DNA decay kinetics in extracellular biological fluids and cell extracts, *Adv. Biosyst.* 4 (2020) 2000057.
- J.A. Kulkarni, P.R. Cullis, R. Van Der Meel, Lipid nanoparticles enabling gene therapies: from concepts to clinical utility, *Nucleic Acid Ther.* 28 (2018) 146–157.
- P.S. Kowalski, A. Rudra, L. Miao, D.G. Anderson, Delivering the messenger: advances in technologies for therapeutic mRNA delivery, *Mol. Ther.* 27 (2019) 710–728.
- S. Ramishetti, I. Hazan-Halevy, R. Palakuri, S. Chatterjee, S. Naidu Gonna, N. Dammes, I. Freilich, L. Kolik Shmuel, D. Danino, D. Peer, A combinatorial library of lipid nanoparticles for RNA delivery to leukocytes, *Adv. Mater.* 32 (2020) 1–8.
- K.J. Kauffman, J.R. Dorkin, J.H. Yang, M.W. Heartlein, F. Derosa, F.F. Mir, O. S. Fenton, D.G. Anderson, Optimization of lipid nanoparticle formulations for mRNA delivery *in vivo* with fractional factorial and definitive screening designs, *Nano Lett.* 15 (2015) 7300–7306.
- A. Akinc, M.A. Maier, M. Manoharan, K. Fitzgerald, M. Jayaraman, S. Barros, S. Ansell, X. Du, M.J. Hope, T.D. Madden, et al., The Onpatro story and the clinical translation of nanomedicines containing nucleic acid-based drugs 14, *Nat. Nanotechnol.*, 2019, pp. 1084–1087.
- J.A. Kulkarni, D. Witzigmann, S. Chen, P.R. Cullis, R. Van Der Meel, Lipid nanoparticle technology for clinical translation of siRNA therapeutics, *Acc. Chem. Res.* 52 (2019) 2435–2444.
- A. Muik, A.K. Wallisch, B. Sängler, K.A. Swanson, J. Mühl, W. Chen, H. Cai, D. Maurus, R. Sarkar, Ö. Türeci, et al., Neutralization of SARS-CoV-2 lineage B.1.1.7 pseudovirus by BNT162b2 vaccine-elicited human sera, *Science* 371 (2021) 1152–1153.
- A. Vogel, et al., BNT162b vaccines protect rhesus macaques from SARS-CoV-2, *Nature* 592 (2021) 283–289.
- U. Sahin, A. Muik, E. Derhovanessian, I. Vogler, L.M. Kranz, M. Vormehr, A. Baum, K. Pascal, J. Quandt, D. Maurus, et al., COVID-19 vaccine BNT162b1 elicits human antibody and TH1 T cell responses, *Nature* 586 (2020) 594–599.
- K. Wu, A.P. Werner, M. Koch, A. Choi, et al., Serum neutralizing activity elicited by mRNA-1273 vaccine, *N.Engl.J.Med.* 384 (2021) 1468–1470.
- L.R. Baden, H.M. El Sahly, B. Essink, K. Kotloff, S. Frey, R. Novak, D. Diemert, S. A. Spector, N. Rouphael, C.B. Creech, et al., Efficacy and safety of the mRNA-1273 SARS-CoV-2 vaccine, *N. Engl. J. Med.* 384 (2021) 403–416.
- A.K. Minnaert, H. Vanluchene, R. Verbeke, I. Lentacker, S.C. De Smedt, K. Raemdonck, N.N. Sanders, K. Remaut, Strategies for controlling the innate immune activity of conventional and self-amplifying mRNA therapeutics: getting the message across, *Adv. Drug Deliv. Rev.* 176 (2021), 113900.
- S.C. Semple, A. Akinc, J. Chen, A.P. Sandhu, B.L. Mui, C.K. Cho, D.W.Y. Sah, D. Stebbing, E.J. Crosley, E. Yaworski, et al., Rational design of cationic lipids for siRNA delivery, *Nat. Biotechnol.* 28 (2010) 172–176.
- S. Liu, Q. Cheng, T. Wei, X. Yu, L.T. Johnson, L. Farbiak, D.J. Siegwart, Membrane destabilizing ionizable phospholipids for organ-selective mRNA delivery and CRISPR-Cas gene editing, *Nat. Mater.* 20 (2021) 701–710.
- K.T. Love, K.P. Mahon, C.G. Levins, K.A. Whitehead, W. Querbes, J.R. Dorkin, J. Qin, W. Cantley, L.L. Qin, T. Racie, et al., Lipid-like materials for low-dose, *in vivo* gene silencing, *Proc. Natl. Acad. Sci. U. S. A.* 107 (2010) 1864–1869.
- D. Zhi, Y. Bai, J. Yang, S. Cui, Y. Zhao, H. Chen, S. Zhang, A review on cationic lipids with different linkers for gene delivery, *Adv. Colloid Interf. Sci.* 253 (2018) 117–140.
- Y. Zhang, C. Sun, C. Wang, K.E. Jankovic, Y. Dong, Lipids and lipid derivatives for RNA delivery, *Chem. Rev.* 121 (2021) 12181–12277.
- G. Sahay, W. Querbes, C. Alabi, A. Eltoukhy, S. Sarkar, C. Zurenko, E. Karagiannis, K. Love, D. Chen, R. Zoncu, et al., Efficiency of siRNA delivery by lipid nanoparticles is limited by endocytic recycling, *Nat. Biotechnol.* 31 (2013) 653–658.
- M.P. Stewart, A. Lorenz, J. Dahlman, G. Sahay, Challenges in carrier-mediated intracellular delivery: moving beyond endosomal barriers, *Wiley Interdiscip. Rev. Nanomed. Nanobiotechnol.* 8 (2016) 465–478.
- J.B. Miller, D.J. Siegwart, Design of synthetic materials for intracellular delivery of RNAs: from siRNA-mediated gene silencing to CRISPR/Cas gene editing, *Nano Res.* 11 (2018) 5310–5337.
- S. Rietwyk, D. Peer, Next-generation lipids in RNA interference therapeutics, *ACS Nano* 11 (2017) 7572–7586.
- R. Kaur, V.W. Bramwell, D.J. Kirby, Y. Perrie, Manipulation of the surface Pegylation in combination with reduced vesicle size of cationic liposomal adjuvants modifies their clearance kinetics from the injection site, and the rate and type of T cell response, *J. Control. Release* 164 (2012) 331–337.
- K. Lappalainen, I. Jääskeläinen, K. Syrjänen, A. Urtti, S. Syrjänen, Comparison of cell proliferation and toxicity assays using two cationic liposomes, *Pharm. Res. An Off. J. Am. Assoc. Pharm. Sci.* 11 (1994) 1127–1131.
- H. Lv, S. Zhang, B. Wang, S. Cui, J. Yan, Toxicity of cationic lipids and cationic polymers in gene delivery, *J. Control. Release* 114 (2006) 100–109.
- S. Sabnis, E.S. Kumarasinghe, T. Salerno, C. Mihai, T. Ketova, J.J. Senn, A. Lynn, A. Bulychchev, I. McFadyen, J. Chan, et al., A novel amino lipid series for mRNA delivery: improved endosomal escape and sustained pharmacology and safety in non-human primates, *Mol. Ther.* 26 (2018) 1509–1519.
- F. Joris, S.C. De Smedt, K. Raemdonck, Small molecules convey big messages: boosting non-viral nucleic acid delivery with low molecular weight drugs, *Nano Today* 16 (2017) 14–29.
- F. Joris, L. De Backer, T. Van de Vyver, C. Bastiancich, S.C. De Smedt, K. Raemdonck, Repurposing cationic amphiphilic drugs as adjuvants to induce lysosomal siRNA escape in nanogel transfected cells, *J. Control. Release* 269 (2018) 266–276.
- T. Van de Vyver, B. Bogaert, L. De Backer, F. Joris, R. Guagliardo, J. Van Hoeck, P. Merckx, S. Van Calenbergh, S. Ramishetti, D. Peer, et al., Cationic amphiphilic drugs boost the lysosomal escape of small nucleic acid therapeutics in a nanocarrier-dependent manner, *ACS Nano* 14 (2020) 4774–4791.
- Z. Fišar, Interactions between tricyclic antidepressants and phospholipid bilayer membranes, *Gen. Physiol. Biophys.* 24 (2005) 161–180.
- S. Schreier, S.V.P. Malheiros, E. De Paula, Surface active drugs: self-association and interaction with membranes and surfactants. *Physicochemical and biological aspects*, *Biochim. Biophys. Acta Biomembr.* 1508 (2000) 210–234.
- R. Kapoor, T.A. Peyear, R.E. Koeppel, O.S. Andersen, Antidepressants are modifiers of lipid bilayer properties, *J. Gen. Physiol.* 151 (2019) 342–356.
- H.M. Britt, A.S. Prakash, S. Appleby, J.A. Mosely, J.M. Sanderson, Lysis of membrane lipids promoted by small organic molecules: reactivity depends on structure but not lipophilicity, *Sci. Adv.* 6 (2020) 1–8.
- R. van der Meel, S. Chen, J. Zaifman, J.A. Kulkarni, X.R.S. Zhang, Y.K. Tam, M. B. Bally, R.M. Schiffelers, M.A. Ciufolini, P.R. Cullis, et al., Modular lipid nanoparticle platform technology for siRNA and lipophilic prodrug delivery, *Small* 17 (2021), 2103025.
- O.S. Fenton, K.J. Kauffman, R.L. McClellan, E.A. Appel, J.R. Dorkin, M.W. Tibbitt, M.W. Heartlein, F. De Rosa, R. Langer, D.G. Anderson, Bioinspired alkenyl amino alcohol ionizable lipid materials for highly potent *in vivo* mRNA delivery, *Adv. Mater.* 28 (2016) 2939–2943.
- J.C. Kaczmarek, K.J. Kauffman, O.S. Fenton, K. Sadler, A.K. Patel, M.W. Heartlein, F. Derosa, D.G. Anderson, Optimization of a degradable polymer-lipid nanoparticle for potent systemic delivery of mRNA to the lung endothelium and immune cells, *Nano Lett.* 18 (2018) 6449–6454.
- R. Verbeke, I. Lentacker, L. Wayteck, K. Breckpot, M. Van Bockstal, B. Descamps, C. Vanhove, S.C. De Smedt, H. Dewitte, Co-delivery of nucleoside-modified mRNA and TLR agonists for cancer immunotherapy: restoring the immunogenicity of immunosilent mRNA, *J. Control. Release* 266 (2017) 287–300.
- I. MacLachlan, *Liposomal formulations for nucleic acid delivery*, *Antisense Drug Technol Princ. Strateg. Appl. Second Ed.* (2007) 237–270.
- K. Buyens, S.C. De Smedt, K. Braeckmans, J. Demeester, L. Peeters, L.A. Van Grunsven, Du De Mollerat, X. Jéu, R. Sawant, V. Torchilin, K. Farkasova, et al., Liposome based systems for systemic siRNA delivery: stability in blood sets the requirements for optimal carrier design, *J. Control. Release* 158 (2012) 362–370.
- J.W. Meisel, G.W. Gokel, A simplified direct lipid mixing lipoplex preparation: comparison of liposomal-, dimethylsulfoxide-, and ethanol-based methods, *Sci. Rep.* 6 (2016) 1–12.
- H. Zhang, S.C. De Smedt, K. Remaut, Fluorescence correlation spectroscopy to find the critical balance between extracellular association and intracellular dissociation of mRNA complexes, *Acta Biomater.* 75 (2018) 358–370.

- [49] G. Sahay, D.Y. Alakhova, A.V. Kabanov, Endocytosis of nanomedicines, *J. Control. Release* 145 (2010) 182–195.
- [50] E. Fröhlich, The role of surface charge in cellular uptake and cytotoxicity of medical nanoparticles, *Int. J. Nanomedicine* 7 (2012) 5577–5591.
- [51] J. Heyes, L. Palmer, K. Bremner, I. MacLachlan, Cationic lipid saturation influences intracellular delivery of encapsulated nucleic acids, *J. Control. Release* 107 (2005) 276–287.
- [52] I.M. Hafez, N. Maurer, P.R. Cullis, On the mechanism whereby cationic lipids promote intracellular delivery of polynucleic acids, *Gene Ther.* 8 (2001) 1188–1196.
- [53] X. Cheng, R.J. Lee, The role of helper lipids in lipid nanoparticles (LNPs) designed for oligonucleotide delivery, *Adv. Drug Deliv. Rev.* 99 (2016) 129–137.
- [54] A.S. Dixon, M.K. Schwinn, M.P. Hall, K. Zimmerman, P. Otto, T.H. Lubben, B. L. Butler, B.F. Binkowski, T. MacHleidt, T.A. Kirkland, et al., NanoLuc complementation reporter optimized for accurate measurement of protein interactions in cells, *ACS Chem. Biol.* 11 (2016) 400–408.
- [55] E. Pottie, A. Cannaert, C.P. Stove, In vitro structure–activity relationship determination of 30 psychedelic new psychoactive substances by means of β -arrestin 2 recruitment to the serotonin 2A receptor, *Arch. Toxicol.* 94 (2020) 3449–3460.
- [56] E. Pottie, D.K. Tosh, Z.G. Gao, K.A. Jacobson, C.P. Stove, Assessment of biased agonism at the A3 adenosine receptor using β -arrestin and miniG α i recruitment assays, *Biochem. Pharmacol.* 177 (2020), 113934.
- [57] E. Pottie, A. Cannaert, K. Van Uytfanghe, C.P. Stove, Setup of a serotonin 2A receptor (5-HT2AR) bioassay: demonstration of its applicability to functionally characterize hallucinogenic new psychoactive substances and an explanation why 5-HT2AR bioassays are not suited for universal activity-based screening, *Anal. Chem.* 91 (2019) 15444–15452.
- [58] O.G. de Jong, D.E. Murphy, I. Mäger, E. Willms, A. Garcia-Guerra, J.J. Gitz-Francois, J. Lefferts, D. Gupta, S.C. Steenbeek, J. van Rheenen, et al., A CRISPR-Cas9-based reporter system for single-cell detection of extracellular vesicle-mediated functional transfer of RNA, *Nat. Commun.* 11 (2020), 1113.
- [59] N.F. Ilahibaks, Z. Lei, E.A. Mol, A.K. Deshantri, L. Jiang, R.M. Schiffelers, P. Vader, J.P.G. Sluijter, Biofabrication of cell-derived nanovesicles: a potential alternative to extracellular vesicles for regenerative medicine, *Cells* 8 (2019) 1509.
- [60] J. Van Hoeck, T. Van de Vyver, A. Harizaj, G. Goetgeluk, P. Merckx, J. Liu, M. Wels, F. Sauvage, H. De Keersmaecker, C. Vanhove, et al., Hydrogel-induced cell membrane disruptions enable direct cytosolic delivery of membrane-impermeable cargo, *Adv. Mater.* 33 (2021) 2008054.
- [61] L. Raes, S. Stremersch, J.C. Fraire, T. Brans, G. Goetgeluk, S. De Munter, L. Van Hoecke, R. Verbeke, J. Van Hoeck, R. Xiong, et al., Intracellular delivery of mRNA in adherent and suspension cells by vapor nanobubble photoporation, *Nano-Micro Lett.* 12 (2020) 185.
- [62] F. Sauvage, V.P. Nguyen, Y. Li, A. Harizaj, J. Sebag, D. Roels, V. Van Havere, K. Peynshaert, R. Xiong, J.C. Fraire, et al., Laser-induced nanobubbles safely ablate vitreous opacities in vivo, *Nat. Nanotechnol.* 17 (2022) 552–559.
- [63] V.P. Nguyen, W. Fan, T. Zhu, W. Qian, Y. Li, B. Liu, W. Zhang, J. Henry, S. Yuan, X. Wang, et al., Long-term, noninvasive in vivo tracking of progenitor cells using multimodality photoacoustic, optical coherence tomography, and fluorescence imaging, *ACS Nano* 15 (2021) 13289–13306.
- [64] V.P. Nguyen, W. Qian, Y. Li, B. Liu, M. Aaberg, J. Henry, W. Zhang, X. Wang, Y. M. Paulus, Chain-like gold nanoparticle clusters for multimodal photoacoustic microscopy and optical coherence tomography enhanced molecular imaging, *Nat. Commun.* 12 (2021), 34.
- [65] M. Wels, D. Roels, K. Raemdonck, S.C. De Smedt, F. Sauvage, Challenges and strategies for the delivery of biologics to the cornea, *J. Control. Release* 333 (2021) 560–578.
- [66] V.P. Nguyen, Y. Li, J. Henry, W. Zhang, X. Wang, Y.M. Paulus, Gold nanorod enhanced photoacoustic microscopy and optical coherence tomography of choroidal neovascularization, *ACS Appl. Mater. Interfaces* 13 (2021) 40214–40228.
- [67] T. Van de Vyver, S.C. De Smedt, K. Raemdonck, Modulating intracellular pathways to improve non-viral delivery of RNA therapeutics, *Adv. Drug Deliv. Rev.* 181 (2022), 114041.